Article
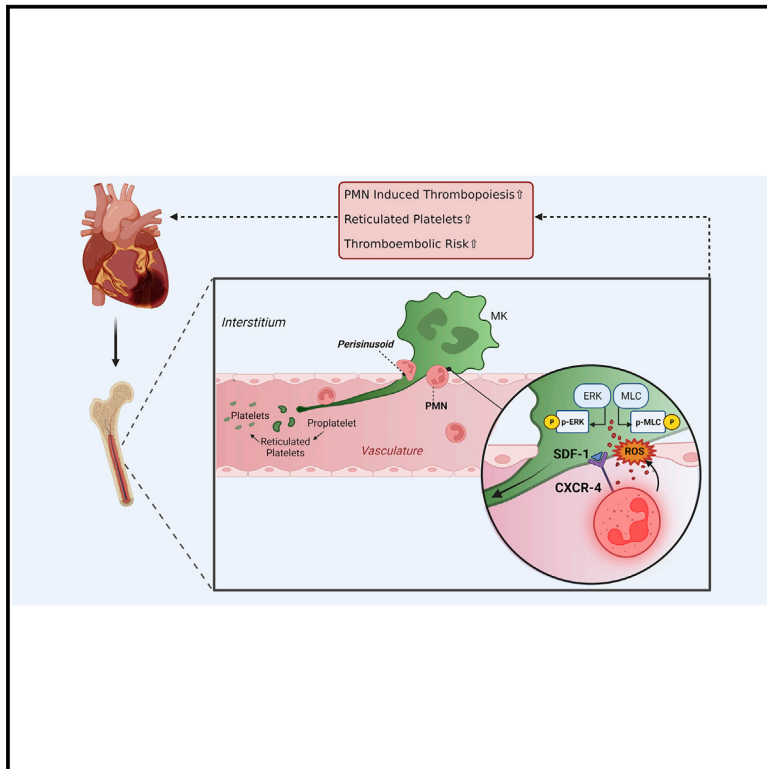
Neutrophil "plucking" on megakaryocytes drives platelet production and boosts cardiovascular disease

Graphical abstract

Authors
Tobias Petzold, Zhe Zhang,
Iván Ballesteros, ..., Christian Schulz,
Andrés Hidalgo, Steffen Massberg

Correspondence
tobias.petzold@med.uni-muenchen.de
(T.P.),
steffen.massberg@
med.uni-muenchen.de (S.M.)

In brief

The importance of megakaryocyte and neutrophil interactions within the bone marrow is insufficiently understood. Petzold and colleagues define neutrophil "plucking"-induced mechanosignaling in megakaryocytes as a regulator of platelet production that boosts cardiovascular diseases.

Highlights

- Plucking of neutrophils on megakaryocyte extensions drives platelet production

- Neutrophils induce mechanosignaling in megakaryocytes via CXCR4 and NOX2

- Neutrophil plucking boosts thrombus burden in thromboinflammatory diseases

CellPress

Article

Neutrophil "plucking" on megakaryocytes drives platelet production and boosts cardiovascular disease

Tobias Petzold,[1,9,15,20,21,*] Zhe Zhang,[1,15,20] Iván Ballesteros,[2] Inas Saleh,[1,9,15] Amin Polzin,[4] Manuela Thienel,[1,9,15]
Lulu Liu,[1,9,15] Qurrat Ul Ain,[1,9,15] Vincent Ehreiser,[1,9,15] Christian Weber,[1,9,15] Badr Kilani,[1,9,15] Pontus Mertsch,[3,12]
Jeremias Götschke,[3,12] Sophie Cremer,[4] Wenwen Fu,[1] Michael Lorenz,[1,15] Hellen Ishikawa-Ankerhold,[1,9,15]
Elisabeth Raatz,[1] Shaza El-Nemr,[1,9,15] Agnes Görlach,[5,9] Esther Marhuenda,[6] Konstantin Stark,[1,9,15] Joachim Pircher,[1,9,15]
David Stegner,[7] Christian Gieger,[8,13,14] Marc Schmidt-Supprian,[16,17,18] Florian Gaertner,[10] Isaac Almendros,[6,11]
Malte Kelm,[4] Christian Schulz,[1,9,15] Andrés Hidalgo,[2,19] and Steffen Massberg[1,9,15,*]

[1]Medizinische Klinik und Poliklinik I, Klinikum der Universität München, Ludwig-Maximilians- University Munich, 81377 Munich, Germany
[2]Program of Cardiovascular Regeneration, Fundación Centro Nacional de Investigaciones Cardiovasculares (CNIC), 28029 Madrid, Spain
[3]Medizinische Klinik und Poliklinik V, Klinikum der Universität München, Ludwig-Maximilians- University Munich, 81377 Munich, Germany
[4]Department of Cardiology, Pulmonology and Vascular Medicine, Cardiovascular Research Institute Düsseldorf (CARID), Medical Faculty of the Heinrich Heine University Düsseldorf, 40225 Düsseldorf, Germany
[5]Experimental and Molecular Pediatric Cardiology, German Heart Center Munich at the Technical University of Munich, 80636 Munich, Germany
[6]Department of Biomedical Sciences, Faculty of Medicine and Health Sciences, University of Barcelona, 08007 Barcelona, Spain
[7]Institute of Experimental Biomedicine, University Hospital Würzburg and Rudolf Virchow Center for Integrative and Translational Bioimaging, 97070 Würzburg, Germany
[8]Research Unit Molecular Epidemiology, Helmholtz Zentrum München - German Research Center for Environmental Health, 85764 Neuherberg, Germany
[9]Partner site Munich Heart Alliance, DZHK (German Centre for Cardiovascular Research), 80802 Munich, Germany
[10]Institute of Science and Technology Austria, 3400 Klosterneuburg, Austria
[11]CIBER de Enfermedades Respiratorias, 28029 Madrid, Spain
[12]Comprehensive Pneumology Center (CPC-M), Member of the German Center for Lung Research (DZL), 81377 Munich, Germany
[13]Institute of Epidemiology, Helmholtz Zentrum München - German Research Center for Environmental Health, 85764 Neuherberg, Germany
[14]German Center for Diabetes Research (DZD), 85764 Neuherberg, Germany
[15]Institute of Surgical Research at the Walter-Brendel-Centre of Experimental Medicine, Klinikum der Universität München, Ludwig-Maximilians- University Munich, 81377 Munich, Germany
[16]Institute of Experimental Hematology, School of Medicine, Technical University Munich, 80333 Munich, Germany
[17]Center for Translational Cancer Research (TranslaTUM), School of Medicine, Technical University of Munich, Munich 81675, Germany
[18]German Cancer Consortium (DKTK) and German Cancer Research Center (DKFZ), 69117 Heidelberg, Germany
[19]Vascular Biology and Therapeutics Program and Department of Immunobiology, Yale University School of Medicine, New Haven, CT 06510, USA
[20]These authors contributed equally
[21]Lead contact
*Correspondence: tobias.petzold@med.uni-muenchen.de (T.P.), steffen.massberg@med.uni-muenchen.de (S.M.)
https://doi.org/10.1016/j.immuni.2022.10.001

SUMMARY

Intravascular neutrophils and platelets collaborate in maintaining host integrity, but their interaction can also trigger thrombotic complications. We report here that cooperation between neutrophil and platelet lineages extends to the earliest stages of platelet formation by megakaryocytes in the bone marrow. Using intravital microscopy, we show that neutrophils "plucked" intravascular megakaryocyte extensions, termed proplatelets, to control platelet production. Following CXCR4-CXCL12-dependent migration towards perisinusoidal megakaryocytes, plucking neutrophils actively pulled on proplatelets and triggered myosin light chain and extracellular-signal-regulated kinase activation through reactive oxygen species. By these mechanisms, neutrophils accelerate proplatelet growth and facilitate continuous release of platelets in steady state. Following myocardial infarction, plucking neutrophils drove excessive release of young, reticulated platelets and boosted the risk of recurrent ischemia. Ablation of neutrophil plucking normalized thrombopoiesis and reduced recurrent thrombosis after myocardial infarction and thrombus burden in venous thrombosis. We establish neutrophil plucking as a target to reduce thromboischemic events.

INTRODUCTION

Platelets and neutrophils cooperate as motile surveillants to maintain host integrity and to protect against sterile and infectious injury. In pathological conditions, however, this liaison of platelets and neutrophils may be harmful, driving thrombo-inflammatory processes that can lead to lethal thrombotic events, such as myocardial infarction (MI), venous thromboembolism (VTE), or stroke (Stark and Massberg, 2021).

Platelets are produced by megakaryocytes (MK) in the bone marrow (BM), which is also where neutrophils arise from myeloid precursors (Stegner et al., 2017). Inside the BM, platelet-releasing MKs reside in the perisinusoidal space, a communication hub that also provides exit and entry points for neutrophils traveling into the blood or returning from the blood to the BM compartment (Itkin et al., 2016). Direct stochastic cellular interactions between MKs and neutrophils in the BM are therefore predicted (Boisset et al., 2018) and were recently described in the rare setting of emperipolesis (Cunin et al., 2019). Yet, we know little about the biological relevance of interactions between MKs and neutrophils in the BM. In particular, it is unclear whether and, if so, how these interactions participate in adverse thromboinflammatory responses that eventually drive thrombotic complications.

Here, we show that circulating neutrophils homing back to the BM "pluck" on perisinusoidal MK extensions, the proplatelets (PPLs). PPLs are thin MK protrusions formed into BM vessels where they are cleaved off into smaller pre-platelets that will finally segregate into young reticulated (i.e. RNA-rich) prothrombogenic platelets (Machlus and Italiano, 2013). We demonstrate that neutrophil plucking accelerates PPL growth and shedding by direct force transmission and by reactive oxygen species (ROS)-transduced mechanosignaling in PPLs. This process depends on CXCR4-directed migration of neutrophils to BM MKs. Neutrophil plucking tunes the release of platelets in the steady state but exacerbates the production of prothrombotic immature platelets following MI, ultimately aggravating post-MI cardiovascular complications.

RESULTS

Neutrophils interact with MKs inside the BM

To characterize interactions between MKs and polymorphonuclear neutrophils inside the BM, we generated *Pf4-cre*(+)/confetti/*Lyz2*-eGFP dual reporter mice and visualized MKs (and their progeny) and neutrophils using multi-photon microscopy of the calvarian bone (Figure 1A). Neutrophils and MKs engaged in close and long-lasting physical contacts in the BM. On average, each MK was in immediate contact with four different neutrophils at any given time. Over 1 h, each MK accumulated a total of eight interactions with an average duration of approximately 13 min (Figures S1A and S1B). When we stratified MKs by their morphology using the sphericity index (SI) to characterize MK maturation (Figure 1B), we found that mature MKs with an irregular shape (SI < 0.5) were less abundant but more likely to form PPLs compared to highly spherical (SI > 0.8) MKs (Figure S1C). Irregular-shaped,multilobulated MKs (SI < 0.5) established interactions with neutrophils more frequently, which were also longer last-

ing (Figures 1C and 1D), irrespective of the total MK surface area (Figure S1D).

Neutrophils boost platelet production by plucking off PPL fragments

As neutrophils preferentially colocalized with PPL-forming MKs, we hypothesized that they might play an active part in platelet production. Dynamic 2-photon microscopy showed that neutrophils preferentially gathered around growing intravascular PPLs and their budding sites at MKs (Figures 1E and 1F). While interacting with PPLs, interstitial and intravascular neutrophils within the perisinusoidal space appeared to "pluck" on PPLs until fragments were shed into the circulation (Figure 1G and Video S1). To define whether neutrophil plucking contributed to PPL shedding, we examined neutrophil-MK interactions *in vitro* using a co-culture model of fetal liver cells (FLCs) and BM-derived neutrophils (Figure 1H). Live cell microscopy showed that neutrophils actively pull on PPLs, applying force that eventually translated into PPL fragmentation (Figure 1I and Video S1). Our imaging data thus showed that neutrophils engage with PPLs by direct physical interactions from their budding stage until they are cleaved off in a process resembling active plucking.

To define the biological relevance of neutrophil plucking for steady state platelet production *in vivo*, we analyzed thrombopoiesis in a mouse model of inducible neutropenia (Figure 2A). Gr-1 antibody treatment induced peripheral neutropenia but did not deplete neutrophils in the BM interstitium and did not bind to platelets or MKs (Figures S1E–S1G). Depletion of circulating neutrophils in *Pf4-cree*(+)/confetti$^{-/-}$/*Lyz2*-eGFP mice led to reduced intravascular and perisinusoidal MK-neutrophil interactions at the PPL budding site (Figures 2B–2D and S1H). At the same time, the number of MKs releasing PPLs was reduced (Figure S1I). A detailed analysis of PPL formation kinetics revealed lower PPL growth speeds and prolonged release times due to repetitive PPL retractions in neutropenic mice (Figure 2E). In addition, PPL release index was reduced after neutrophil depletion (ND) compared to control conditions, while PPL length was unaffected (Figure S1J and Video S1). PPL growth and fragmentation was also reduced in pan-neutropenic *Mrp8-cre*(+)/iDTR mice (Casanova-Acebes et al., 2018) lacking the intravascular, perisinusoidal, and interstitial neutrophil pool (Figures S1K and S1L). When we rescued the circulation neutrophil pool of *Mrp8-cre*(+)/iDTR mice by adoptive transfer of Ly6G-labeled neutrophils (Figure 2F), this restored PPL plucking by neutrophils and accelerated PPL growth and fragmentation (Figures 2G, 2H, and Video S1). Together, this indicates that plucking neutrophils promote PPL growth and fragmentation (Figure 2I).

Neutropenia blunts thrombopoiesis in the steady state

To test the role of neutrophil plucking for platelet homeostasis in steady state, we characterized platelet counts in both models of inducible neutropenia. Gr-1-mediated depletion of circulating neutrophils caused a reduction in circulating platelet numbers (i.e. platelet counts: −32.6%), which was due to reduced production of young, reticulated platelets (reticulated platelet counts: −49.6% vs. control treatment), while platelet lifespan, MK numbers, size, and ploidy were unaffected (Figures 3A and S2A–S2C). Gr-1-induced neutropenia also blunted recovery of
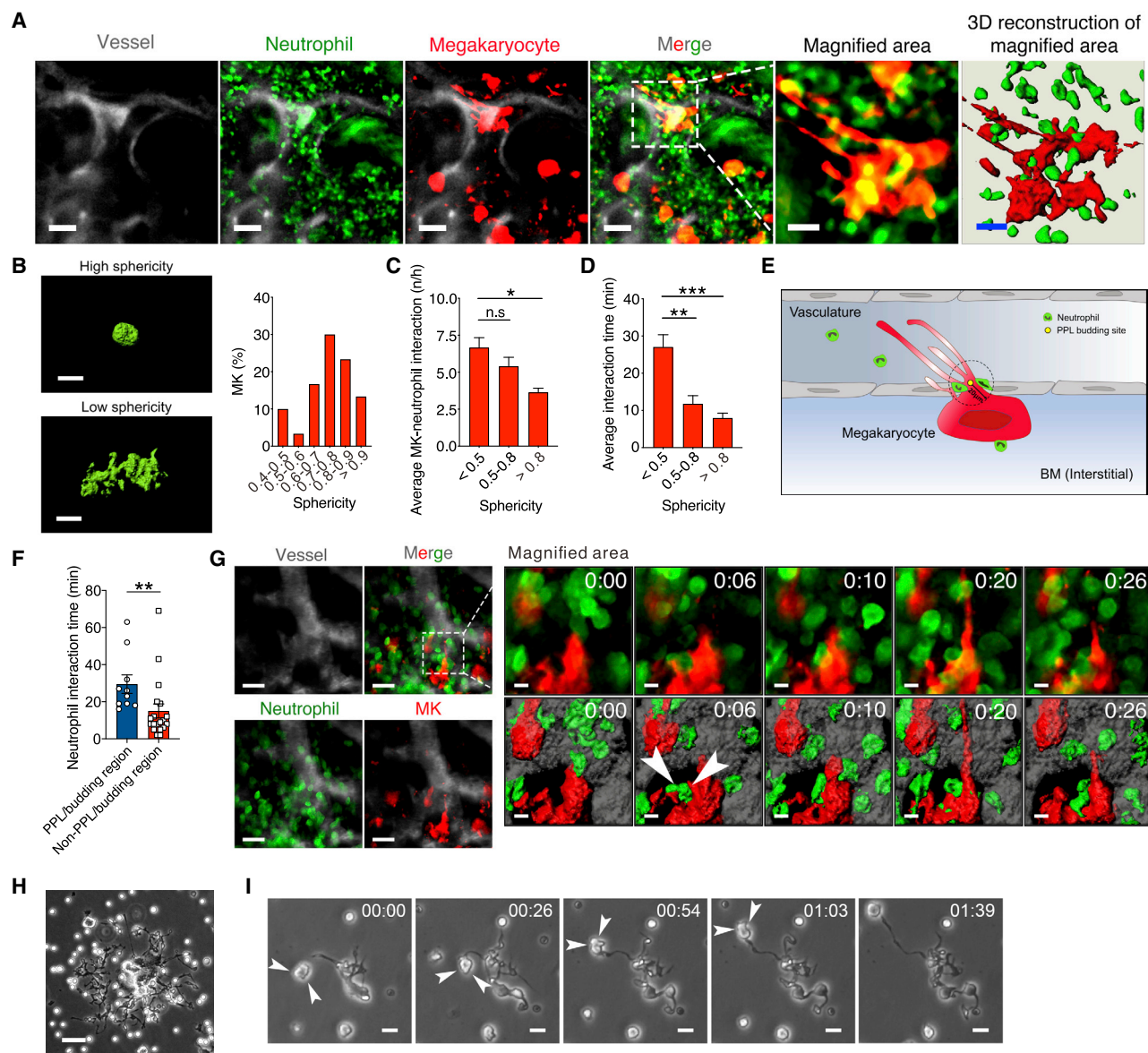
Figure 1. Neutrophil plucking on PPL-forming MKs

(A) Two-photon imaging of thrombopoiesis inside BM in dual reporter mice (*Pf4-cre*(+)/ Confetti$^{-/-}$/*Lyz2*-eGFP). Representative images from 4 independent experiments of MK (multicolor here shown in red) – neutrophil (green) interactions within the BM and a 3D image reconstruction of the magnified area are shown. Scale bars represent 40 μm or 10 μm (magnified area), respectively.

(B) MK characterization by sphericity index. Representative images from 4 independent experiments of low and high sphericity MKs are shown (bar represents 20 μm). Frequency distributions of MKs' sphericity indices within the BM are shown (n = 4 animals per group, 29 MKs were observed and analyzed over the time frame of 1 h).

(C and D) *In vivo* video analyses quantifying MK-neutrophil interactions and interaction times by sphericity index. (C) Frequency distribution of MK-neutrophil (i.e. individual cells) interactions and (D) interaction times over 1 h are shown (n = 4 animals per group, 7 videos per group).

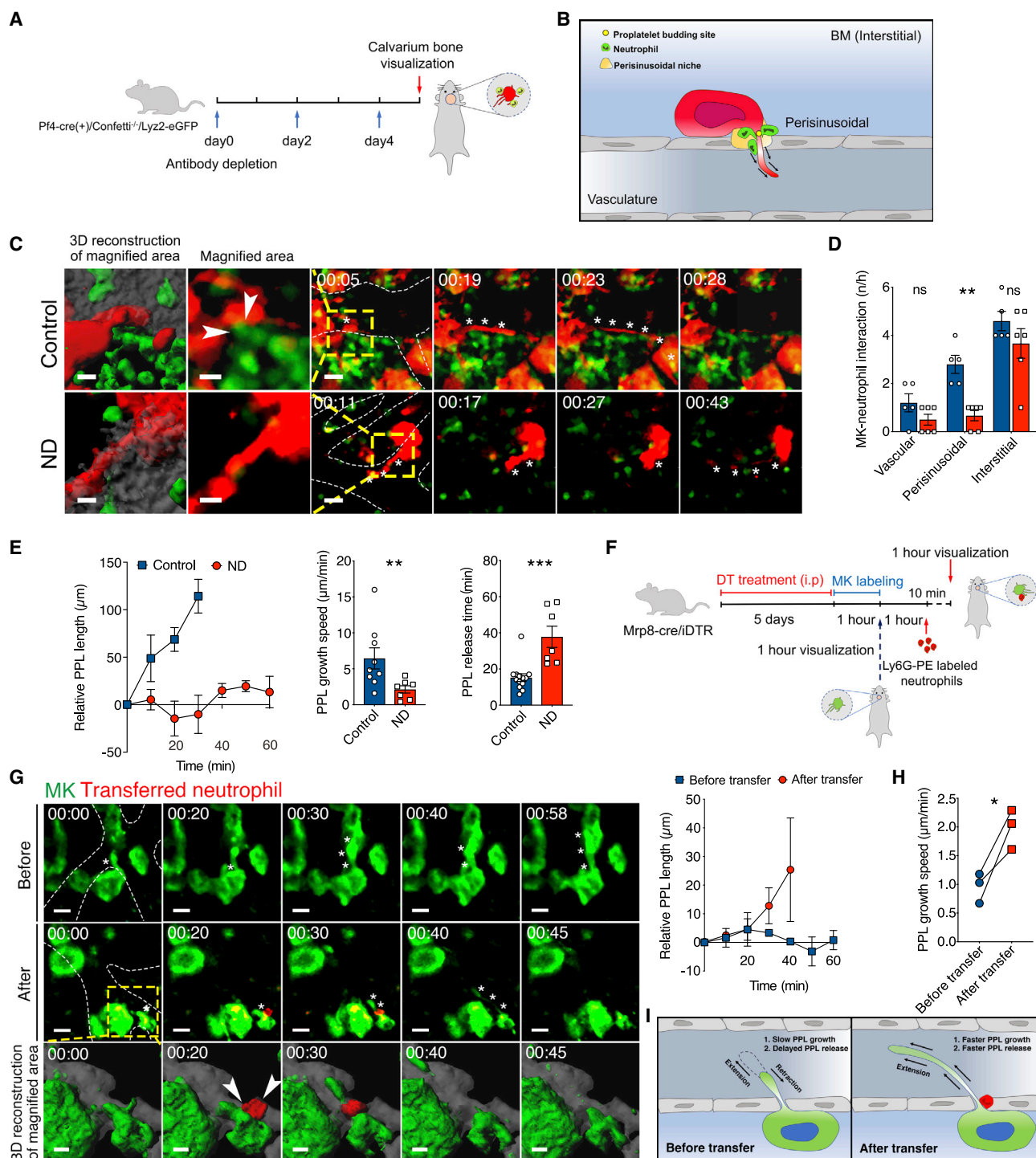(E) Scheme of MK-neutrophil interactions during thrombopoiesis.

(F) Analysis of neutrophil interaction times at the PPL/budding region or Non-PPL/budding region of MKs, symbols indicate individual neutrophils (analysis from 4 animals).

(G) Image series and 4D reconstruction of neutrophil plucking on PPL-forming MK around the PPL budding site is shown. White arrows indicate plucking neutrophil. Scale bars represent 40 μm (overview image) or 5 μm (magnified area), respectively, timeline is indicated.

(H) Brightfield microscopy of MK-neutrophil co-culture is shown. Scale bar represents 20 μm.

(I) Neutrophil plucking during PPL elongation is visualized by time lapse imaging. Arrows indicate plucking neutrophil. Scale bar represents 5 μm. Bars represent mean ± SEM; symbols indicate individual animals; p values are indicated, *<0.05, **<0.01, ***<0.001, ****<0.0001, n.s. not significant. P values were determined using unpaired Student's t test (F), one-way (C, D) ANOVA multigroup test. Please see also Figure S1.

Figure 2. Neutrophil plucking accelerates PPL growth and release during thrombopoiesis

(A–E) Analysis of MK-neutrophil interaction in Gr-1-treated neutropenic and control-antibody-treated dual reporter mice (*Pf4-cre*(+)/Confetti$^{-/-}$/ *Lyz2*-eGFP) by two-photon microscopy.

(A) Scheme of imaging setup in neutropenic mice.

(B) Localization of the interstitial, perisinusoidal, and intravascular BM compartment to further characterize MK-neutrophil interactions.

(C) Image sequence showing PPL formation under neutropenic conditions. White arrows indicate PPL-plucking neutrophil around the budding site. Asterisks indicate PPLs, dashed lines show vasculature, yellow box indicates magnified area. Scale bar represents 5 μm (magnified area) and 20 μm, timeline (min) is indicated.

(D) Quantification of interaction frequencies within BM compartments (control: n = 4 animals, ND: n = 3 animals, symbols indicate single MKs).

(legend continued on next page)

platelet counts in a model of immune thrombocytopenia (Figure S2D). To exclude that Gr-1 treatment reduced platelet production by off-target effects, including depletion of Ly6C-expressing cells beyond neutrophils, we injected Gr-1 into Ly6G-deficient (and thus Gr-1-resistant) catchup mice (Hasenberg et al., 2015). Homozygous, but not heterozygous, catchup mice were protected from neutropenia and showed normal platelet counts upon antibody treatment (Figures S2E and S2F). Pan-neutropenic *Mrp8-cre*(+)/iDTR mice showed a similar decrease in platelet (i.e. platelet count: −25.7% vs. control) and reticulated platelet counts (i.e. reticulated platelet count: −20.8% vs. control) (Figure 3B). Similar to Gr-1 depletion, this was due to reduced platelet production, while platelet lifespan, MK numbers, size, and maturity (i.e. ploidy) were unaffected (Figures S2G–S2I). When we infused α-GPIb antibody to induce immune thrombocytopenia, subsequent platelet recovery was slower and incomplete in pan-neutropenic mice compared to controls (Figure S2J).

To additionally determine whether alterations of the BM interstitial cytokine milieu account for the differences in platelet production in mice lacking circulating neutrophils, we quantified cytokine amounts following Gr-1 treatment. Yet, concentrations of known regulators of thrombopoiesis including thrombopoietin and Il-1α (Noetzli et al., 2019) were not altered in neutropenic compared to control mice (Figure S2K). Changes in interstitial cytokine composition are therefore unlikely to contribute to the regulation of platelet production by intravascular neutrophils.

CXCR4-driven tropism orchestrates thrombopoiesis

To resolve the molecular mechanism of platelet production by neutrophil plucking, we used *in vitro* co-culture. For quantification of *in vitro* thrombopoiesis we measured CD61+ CD42d+ platelet particles (PP) released from PPLs in the culture supernatants (Figure S2L). The presence of neutrophils, but not of CD3+ T cells, CD19+ B cells, or monocytes, boosted PP production to a similar extent as sphingosine-1 phosphate (Figure 3C), a known inducer of thrombopoiesis (Zhang et al., 2012). Analysis of CD3-deficient mice lacking T cells (Sommers et al., 2000), B-cell-depleted *Cd19-cre* iDTR mice (Demircik et al., 2013), *Rag1*−/− mice lacking B and T cells (Mombaerts et al., 1992), and monocyte-depleted mice following CCR2 depletion antibody (Mack et al., 2001) treatment for 5 days did not show altered platelet or reticulated platelet counts (Table 1). Together these data show that immune cell control of thrombopoiesis is cell type specific and restricted to neutrophils.

Neutrophils were able to trigger *in vitro* thrombopoiesis only when we allowed direct physical interaction with MKs, but not when we separated both cell types in a trans-well chamber (Figure 3C). Consistently, supernatants from phorbol 12-myristate 13-acetate (PMA) activated neutrophils did not affect PP release (Figure 3C). Time-lapse imaging suggested that plucking neutrophils applied force to PPLs to promote PP release. To test this, we used small molecule inhibitors to interfere with neutrophil cytoskeleton dynamics and myosin dependent force generation. Pretreatment of neutrophils with cytochalasin D and blebbistatin abolished PP release, indicating that neutrophil plucking requires neutrophil mechanotransduction (Figure 3D).

Next, we performed a receptor screening approach including a set of neutrophil receptors known to mediate platelet interactions. We found that CXCR4-deficient neutrophils isolated from *Mrp8-cre*(+)/*Cxcr4*Δ/Δ mice (Adrover et al., 2019; Casanova-Acebes et al., 2013) failed to increase PP yield compared to wild-type neutrophils (Figure 3E). Neutrophil-driven thrombopoiesis was also abolished following CXCR4 inhibition by AMD3100. In addition, we found an effect for beta1-integrins and integrin activator kindlin-III, required for neutrophil migration *in vitro* and neutrophil adhesion *in vivo*. In contrast, absence or inhibition of PSGL-1, β2 integrin, CD41, or CD40L did not affect neutrophil-induced thrombopoiesis (Figures 3E and S2M).

MKs express high amounts of the CXCR4 ligand stromal-cell-derived factor 1 (SDF-1/CXCL-12) on their surfaces (Massberg et al., 2006) (Figures S3A and S3B). We therefore focused on CXCR4 and analyzed whether ablation of *Cxcr4* on neutrophils impacted their ability to pluck on PPL-forming MKs. First, we adoptively transferred CXCR4-deficient neutrophils isolated from *Mrp8-cre*(+)/*Cxcr4*Δ/Δ/GFP mice or *Mrp8-cre*(−)/*Cxcr4*fl/fl/GFP control neutrophils into C57BL/6 recipients (Figure 3F). Whole-mount confocal microscopy analysis showed that the majority of adoptively transferred wild-type neutrophils localized in close proximity to MKs (Figures 3F and 3G). In contrast, *Cxcr4*-deficient neutrophils were less likely to enter the BM, as reported (Adrover et al., 2019), and were distributed randomly throughout the interstitial space without obvious preference for the MK microenvironment. Thus, to test whether defective homing of neutrophils into the perisinusoidal space translated into changes in thrombopoiesis *in vivo*, we analyzed *Mrp8-cre*(+)/*Cxcr4*Δ/Δ mice. BM imaging demonstrated that the pool of plucking neutrophils in direct proximity (<20 μm) to the PPL budding sites was drastically reduced in *Mrp8-cre*(+)/*Cxcr4*Δ/Δ mice, while neutrophil counts in peripheral blood were increased compared to control littermates (Figures 3H, 3I, S3C, and S3D). Reduced PPL plucking translated into reduced PPL growth speeds and prolonged release times without affecting PPL lengths (Figures 3J and S3E). In agreement with these findings, we observed reduced platelet and reticulated platelet counts in *Mrp8-cre*(+)/*Cxcr4*Δ/Δ compared to control mice (i.e. platelet

(E) Analysis of PPL kinetics. Relative PPL length of individual PPLs (control: 3 PPLs; ND: n = 2PPLs), PPL growth speed, and release time (control: n = 4 animals, ND: n = 3 animals) are shown.

(F–H) Neutrophil rescue by adoptive transfer in neutropenic *Mrp8-cre*(+)/iDTR mice.

(F) Treatment scheme is shown.

(G) Representative image series of 3 independent experiments and 3D reconstruction of PPL release in mice before and after neutrophil transfer, scale bars represent 15 μm. Analysis of PPL kinetics. Relative length of individual PPLs is shown before and after neutrophil transfer (before: n = 5 PPLs; after: n = 3 PPLs).

(I) Summarizing scheme of adoptive transfer experiments is shown.

(H) Quantification of PPL growth speed before and after neutrophil transfer (n = 3 animals per group). Bars represent mean ± SEM, symbols indicate individual animals or MKs; p values are indicated, *<0.05, **<0.01, ***<0.001, n.s. not significant. P values were determined using unpaired (E) or paired (H) Student's t test and two-way (D) ANOVA multigroup test. Please see also Figures S1 and S2.
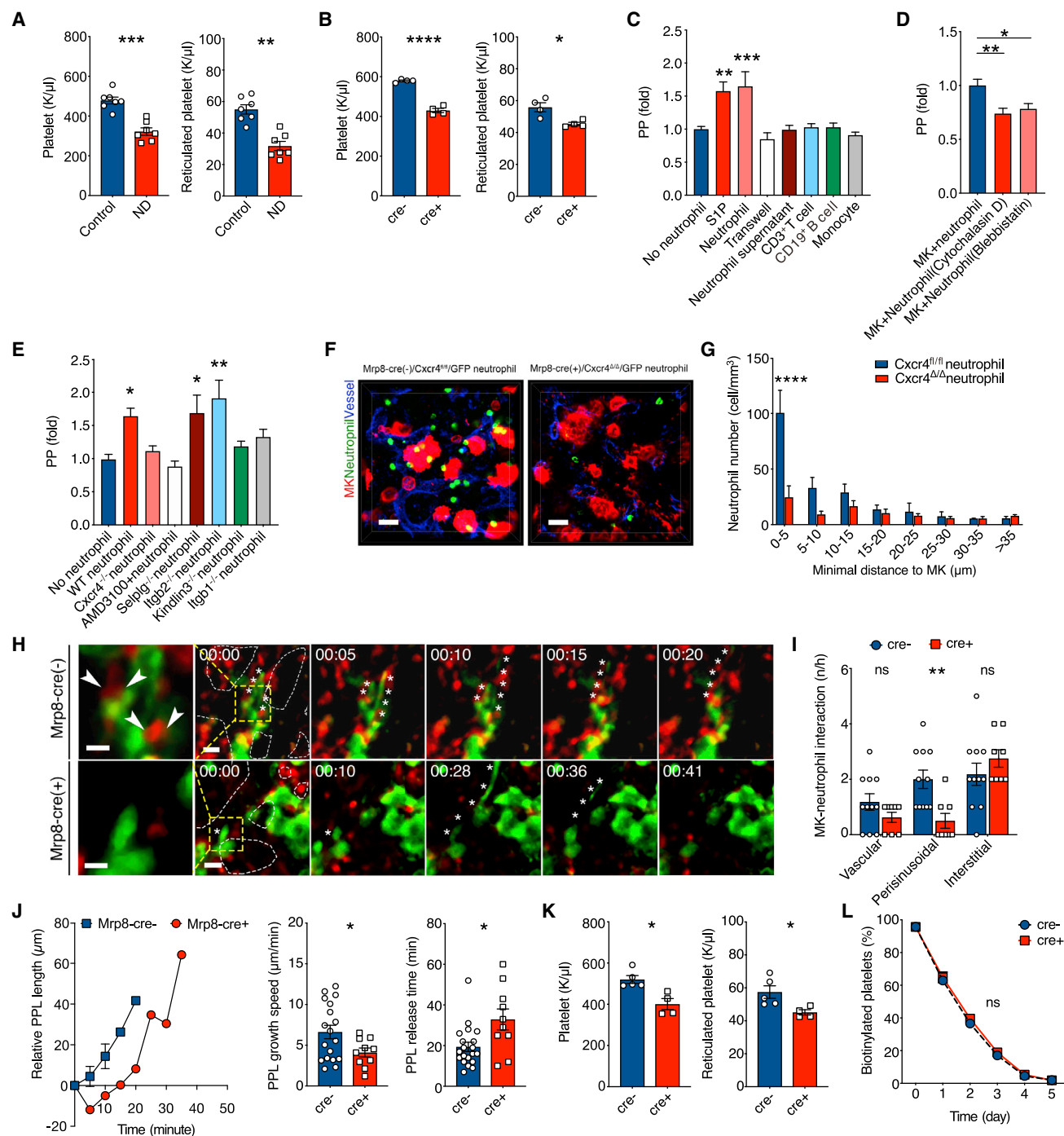
Figure 3. Neutrophil-expressed CXCR4 regulates neutrophil plucking and platelet production

(A and B) Quantification of platelet and reticulated platelet counts in two murine models of neutropenia.

(A) Platelet and reticulated platelet counts in a model of Gr-1-antibody-induced neutropenia are shown (n = 7 animals per group).

(B) Platelet and reticulated platelet counts in a model of diphtheria-toxin-induced neutropenia in Mrp8-Cre/Rosa26iDTR mice (n = 4 animals per group) are shown.

(C–E) *In vitro* thrombopoiesis in a co-culture of primary-fetal-liver-cell-derived MKs and BM-derived neutrophils.

(C) Quantification of platelet particles (PPs) within supernatants by flow cytometry 6 h after addition of neutrophils, sphingosine-1-phosphate (10 nM), neutrophils separated by trans-well, pan CD3^{+} T cells, CD19^{+} B cells, monocytes, or neutrophil supernatants following PMA stimulation (no neutrophil: n = 6, neutrophil: n = 6, S1P: n = 5, trans-well: n = 5, CD3^{+} T cells: n = 5, CD19^{+} B cells: n = 4, monocytes: n = 4, neutrophil supernatant: n = 3).

(D) Analysis of PP production within co-culture supernatants after neutrophil treatment with actin polymerization inhibitor (cytochalasin D)- or myosin inhibitor (blebbistatin)-treated neutrophils. PP release was determined by flow cytometry 6 h after co-culturing (n = 3).

count: −20.7%; reticulated platelet count: −17.4%; vs. control; Figure 3K). In contrast, platelet life span, MK numbers, MK maturity, and platelet neutrophil aggregates were not affected (Figures 3L, S3F, and S3G). Likewise, in *Pf4-cre*(+)/ *Cxcl12*^{−/−} mice that do not express the CXCR4 ligand CXCL12 on MKs, we found reduced neutrophil homing to MKs (Figures S3H and S3I) and reduced platelet production with lower numbers of platelets and reticulated platelets (i.e. platelets: −14.8%; reticulated platelets: −24.4%; vs. control), while platelet lifespan was unaffected (Figures S3J and S3K). This indicates that the CXCR4-CXCL12 axis mediates neutrophil tropism towards MKs and is essential for neutrophil-assisted thrombopoiesis in steady-state conditions. CXCR4-CXCL12 neutrophil-MK interactions supported platelet replenishment in situations of enhanced platelet consumption, as recovery of platelet counts was delayed and incomplete in *Mrp8-cre* (+)/*Cxcr4*[Δ/Δ] mice compared to controls in a model of immune thrombocytopenia (Figure S3L).

Neutrophil-derived ROS drive thrombopoiesis

To investigate the underlying mechanisms of how plucking neutrophils drive platelet production, we tested whether they were capable of transducing direct molecular signals to PPL-forming MKs, orchestrating platelet release. We focused on NADPH-derived ROS. To investigate the role of neutrophil-derived ROS, we transplanted BM from *Cybb*^{−/−} mice (Pollock et al., 1995) into lethally irradiated wild-type recipient mice. *Cybb*^{−/−} chimera had reduced platelet and reticulated platelet counts (Figures S4A and S4B) with unaltered platelet life span compared to control chimeras (Figure S4C). In addition to neutrophils, monocytes and B cells express NOX2, while it is not expressed by MKs (McCrann et al., 2009). However, NOX2-expressing monocytes and B cells did not induce thrombopoiesis (Table 1), suggesting that lack of NOX2 in neutrophils is responsible for the platelet phenotype in *Cybb*^{−/−} chimera. *In vivo* visualization of platelet production revealed attenuated PPL production, while MK-neutrophil interactions were not affected (Figures S4D–S4G and Video S1). MK and neutrophil counts within the BM were increased in NOX2 null chimeras, indicating a regulatory function of NOX2 in MK and neutrophil production (Figures S4H and S4I). Mice treated with the ROS scavenger N-acetylcysteine recapitulated the findings obtained in *Cybb*^{−/−} chimera (i.e. platelets: −13.1%; reticulated platelets: −18.1%;

vs. control treatment) (Figures S4J–S4N). *In vitro* inhibition of NADPH oxidase by apocynin or genetic silencing of NADPH oxidase in *Cybb*^{−/−} as well as *Cyba*[mt/mt] neutrophils (Nakano et al., 2008), which are unable to release superoxide anions and to generate H_2O_2 (Pollock et al., 1995), abolished neutrophil-driven thrombopoiesis. A similar response was found after degradation of extracellular ROS in the presence of catalase and superoxide dismutase (SOD; Figures 4A and S4O). We found that interactions with neutrophils promoted intracellular ROS production (Figures 4B and S4P) and activated MLC and ERK signaling by phosphorylation in MKs, both of which are required for MK maturation, PPL formation (Mazharian et al., 2009), and proper PP release (Chang et al., 2007) (Figure 4C). In addition, neutrophils showed a similar ROS response when we incubated with the CXCR4 ligand CXCL12 (Figure S4Q). Inhibition of either ERK or MLC, even in the absence of neutrophils, abolished PP release (Figure S4R). To gain a better spatial resolution of p-MLC signaling within MKs, we used confocal microscopy. In analogy to immunoblotting, we found elevated p-MLC mean fluorescence intensity (MFI) values in the presence of neutrophils that were accentuated within PPLs compared to the cell body (Figures 4D–4F). This finding aligned with earlier data describing accumulation of p-MLC within the cytoplasmic swelling and at the PPL tip of the forming PPL (Chang et al., 2007).

To evaluate the potential relevance of neutrophil-driven thrombopoiesis in human probands, we analyzed a GWAS dataset obtained from 408,112 individuals (Vuckovic et al., 2020). Focusing on neutrophil migration and ROS production, we identified leukocyte-specific genetic variants for leukocyte integrin subunit LFA-1(rs34114657) and myeloperoxidase (MPO; rs2526378), as well as leukocyte- and MK-expressed CXCR4 (rs11679328), SIRPA (rs6045612), LYN (rs12676105), JAK2 (rs7865719), CYBA (rs556088070), and SHP2 (rs11066283) that associate with platelet counts (Table S1). While correlative, these data pointed to similar mechanisms at play in humans.

In summary, the CXCR4-CXCL12 axis mediates MK tropism of neutrophils that "pluck" on MK to drive PPL growth and release by direct force transmission and induction of ROS-dependent mechanosignaling (Figure 4G).

Neutrophils drive thrombopoiesis in MI

Constant delivery of platelets is essential for physiological blood cell homeostasis, yet it may be detrimental in the context of

---

(E) Quantification of PPs within supernatants by flow cytometry 6 h after addition of indicated receptor-deficient neutrophils or inhibitor (no neutrophil: n = 5; neutrophil: n = 5; *Selplg*: n = 5; *Itgb2*^{−/−}: n = 5; *Cxcr4*^{−/−}: n = 3; AMD3100 (0.5 μg/ml): n = 3; *Itgb1*^{−/−}: n = 3; Kindlin3^{−/−}: n = 3).

(F) Adoptive transfer experiments of *Cxcr4*^{fl/fl}-expressing or *Cxcr4*[Δ/Δ] neutrophils in C57BL/6 mice. Representative 3D reconstruction pictures from 3 independent experiments of whole-mount-stained bones are shown (right, scale bar represents 20 μm).

(G) Minimal MK-neutrophil distance between MKs and neutrophils (n = 3 animals per group).

(H–J) *In vivo* analysis of thrombopoesis in *Mrp8-cre/Cxcr4*^{fl/fl} mice.

(H) Time lapse analysis thrombopoesis *in vivo*. White arrows indicate neutrophil plucking on PPL budding sites. Asterisks indicate PPLs. Timeline (min) is indicated and dashed lines show vasculature, yellow box indicates magnified area. Scale bar represents 5 μm (magnified area) or 20 μm.

(I) *In vivo* imaging analysis in dual-antibody-labeled *Mrp8-cre/cxcr4* mice. Analysis of interaction frequencies within different compartments (*Mrp8-cre*[−]: n = 4 animals; *Mrp8-cre*[+]: n = 3 animals),

(J) Analysis of PPL kinetics. Relative length of individual PPLs (*Mrp8-cre*[−]: n = 3 PPLs; *Mrp8-cre*[+]: n = 1 PPL), PPL growth speed, and release time (*Mrp8-cre* [−]: n = 3 animals; *Mrp8-cre*[+] n = 3 animals) are shown.

(K and L) Characterization of *Mrp8-cre/Cxcr4* mice. Quantification of (K) platelet and reticulated platelet counts (*Mrp8-cre*[−]: n = 5 animals; *Mrp8-cre*[+] n = 4 animals) as well as (L) platelet life span (n = 3 animals per group) are shown. Bars represent mean ± SEM; symbols indicate individual animals or MKs; p values are indicated, *<0.05, **<0.01, ***<0.001, ****<0.0001, n.s. not significant. P values were determined with unpaired Student's t test (A, B, J (right), and K), or one-way (C, D, and E) or two-way (G, I, and L) ANOVA multigroup test. Please see also Figure S3.

Table 1. Characterization of leukocyte-subpopulation-deficient mouse models (related to Figure 3)

	Blood							Bone marrow			
	WBC (10³/µL)	Platelet (10³/µL)	Reticulated platelet (10³/µL)	Neutrophil (10³/µL)	Monocyte (10³/µL)	B cell (10³/µL)	T cell (10³/µL)	Neutrophil (10³/µL)	Monocyte (10³/µL)	B cell (10³/µL)	T cell (10³/µL)
Cd19_iDTR(−)	4.69 ± 0.44	1023 ± 106.22	136.11 ± 11.58	1.42 ± 0.35	0.15 ± 0.06	1.02 ± 0.19	1.45 ± 0.33	15.62 ± 1.67	2.59 ± 0.71	8.51 ± 2.49	0.97 ± 0.36
Cd19_iDTR(+)	3.06 ± 0.23*	1113.25 ± 36.55	136.60 ± 15.43	1.41 ± 0.39	0.16 ± 0.04	0.05 ± 0.04*	1.17 ± 0.6	12.42 ± 0.79	1.74 ± 0.71	0.41 ± 0.06*	0.76 ± 0.4
Cd3e-WT	4.85 ± 0.51	884 ± 12.67	115.84 ± 13.37	1.12 ± 0.19	0.14 ± 0.07	0.75 ± 0.05	2.21 ± 0.58	14.83 ± 1.71	1.83 ± 1.52	9.65 ± 1.04	1.16 ± 0.18
Cd3e-KO	2.54 ± 0.49*	885 ± 43.87	112.18 ± 6.86	0.88 ± 0.16	0.15 ± 0.04	0.83 ± 0.48	0.01 ± 0.005*	12.88 ± 0.84	1.32 ± 0.36	12.39 ± 1.68	0.25 ± 0.09*
Isotype control	3.49 ± 0.45	999.75 ± 53.1	130.11 ± 6.04	0.75 ± 0.31	0.22 ± 0.08	1.3 ± 0.15	0.92 ± 0.153	15.58 ± 2.84	1.20 ± 0.33	10.14 ± 1.26	1.3 ± 0.14
CCR2 antibody	4.9 ± 1.27	942.5 ± 117.76	140.27 ± 16.11	0.95 ± 0.37	0.005 ± 0.004*	2.12 ± 0.31	1.44 ± 0.41	14.92 ± 1.88	1.10 ± 0.19	10.59 ± 0.90	1.02 ± 0.15
Rag1-WT	6.32 ± 1.05	1118 ± 148.9	93.34 ± 12.15	0.47 ± 0.06	0.19 ± 0.07	2.21 ± 0.78	1.58 ± 0.40	n.a.			
Rag1-KO	1.44 ± 0.29****	1084.8 ± 294.9	97.89 ± 25.67	0.36 ± 0.09	0.10 ± 0.04	0.002 ± 0.001*	0.03 ± 0.01*	n.a.			

White blood counts (WBC) and platelet numbers were quantified by blood counter analysis. Reticulated platelets and leukocyte subsets in blood and bone marrow were analyzed using flow cytometer (n = 4–5 animals per group). Table shows mean ± SD; p values are indicated: p < 0.05 (*), p < 0.0001 (****). P values were determined by unpaired Student's t test.
* Indicates p value < 0.05, ****p value < 0.0001; n.a. Not available.
# Cd19-iDTR mice received 3 consecutive days of diphtheria toxin treatment, i.p., 10 ng/g per day; For monocyte depletion, C57BL/6 mice received 5 consecutive days CCR2 antibody or isotype control antibody, i.p.,20 µg/day.

thrombotic cardiovascular diseases. In MI, increased fractions of immature platelets in blood are associated with increased risk of recurrent ischemia, one-year mortality, and elevated risk of recurrent thrombotic events after an index MI (Cesari et al., 2013). Immature platelets show a prothrombotic phenotype with elevated expression of central adhesion and signaling molecules (Bongiovanni et al., 2019). Compared to mature platelets, we detected increased surface amounts of collagen receptor GPVI and active GPIIb/IIIA on immature murine platelets (Figures S5A and S5B). We also found increased reactivity of immature platelets with increased agonist-induced expression of CD40L, active GPIIb/IIIA, and P-selectin, all known to drive thrombus formation (Figures S5A and S5B).

Analysis of ST-elevation myocardial infarction (STEMI) patients undergoing percutaneous coronary intervention (PCI; baseline characteristics are shown in Table S2) revealed a transient increase in reticulated platelet counts (i.e. reticulated platelet counts +50.7%), returning to the amounts found in patients with stable coronary artery disease at day 5 (Figure 5A). CXCR4 expression on peripheral blood neutrophils showed a similar transient increase (Figure 5B).

To characterize the role of neutrophil-driven thrombopoiesis after MI we used a mouse model of myocardial ischemia reperfusion (I/R) injury closely resembling the situation in human MI patients. When we adoptively transferred neutrophils, we found a preferential localization of transferred neutrophils around BM-resident MKs in MI mice compared to sham (Figure 5C). Imaging of murine BM 48 h post MI, we observed increased numbers of PPL-plucking neutrophils in the perisinusoidal space associated with augmented PPL growth speeds and faster PPL release times compared to sham treatment (Figures 5D–5F and Video S2). Consistent with our observation in MI patients, we found elevated platelet and reticulated platelet counts 48 h after mouse MI (i.e. platelet counts: +13.1%; reticulated platelet counts: +29.6%; vs. sham treatment) (Figure 5H), while MK numbers and maturity within the BM were unchanged (Figure S5C). MI mice revealed elevated peripheral neutrophil counts with increased CXCR4 surface expression similar to MI patients, paralleled by increased ROS amounts (Figures S5D, 5I, and 5J). These data show that neutrophil plucking contributes to disproportionate, prothrombogenic platelet production during MI.

CXCR4-driven thrombopoiesis drives recurrent arterial thrombosis and VTE

To study the consequences of increased numbers of circulating prothrombotic immature platelets, we induced MI in mice and analyzed subsequent thrombus formation in distant vascular beds outside the coronary arteries. We used a dual-labeled antibody assay to distinguish younger (<12 h of age) from older platelets. We found that already in the absence of a previous MI, young, reticulated platelets were preferentially recruited into microvascular mesenteric artery thrombus with higher fractions when compared to total blood. A preceding MI boosted the number of immature platelets in the blood and to a similar extent also within the distant thrombus (Figures 6A and 6B and Video S2). When we induced arterial thrombosis of the common carotid artery, the rate of vessel occlusions (Figure 6C and Video S2), thrombus size, and overall thrombus burden
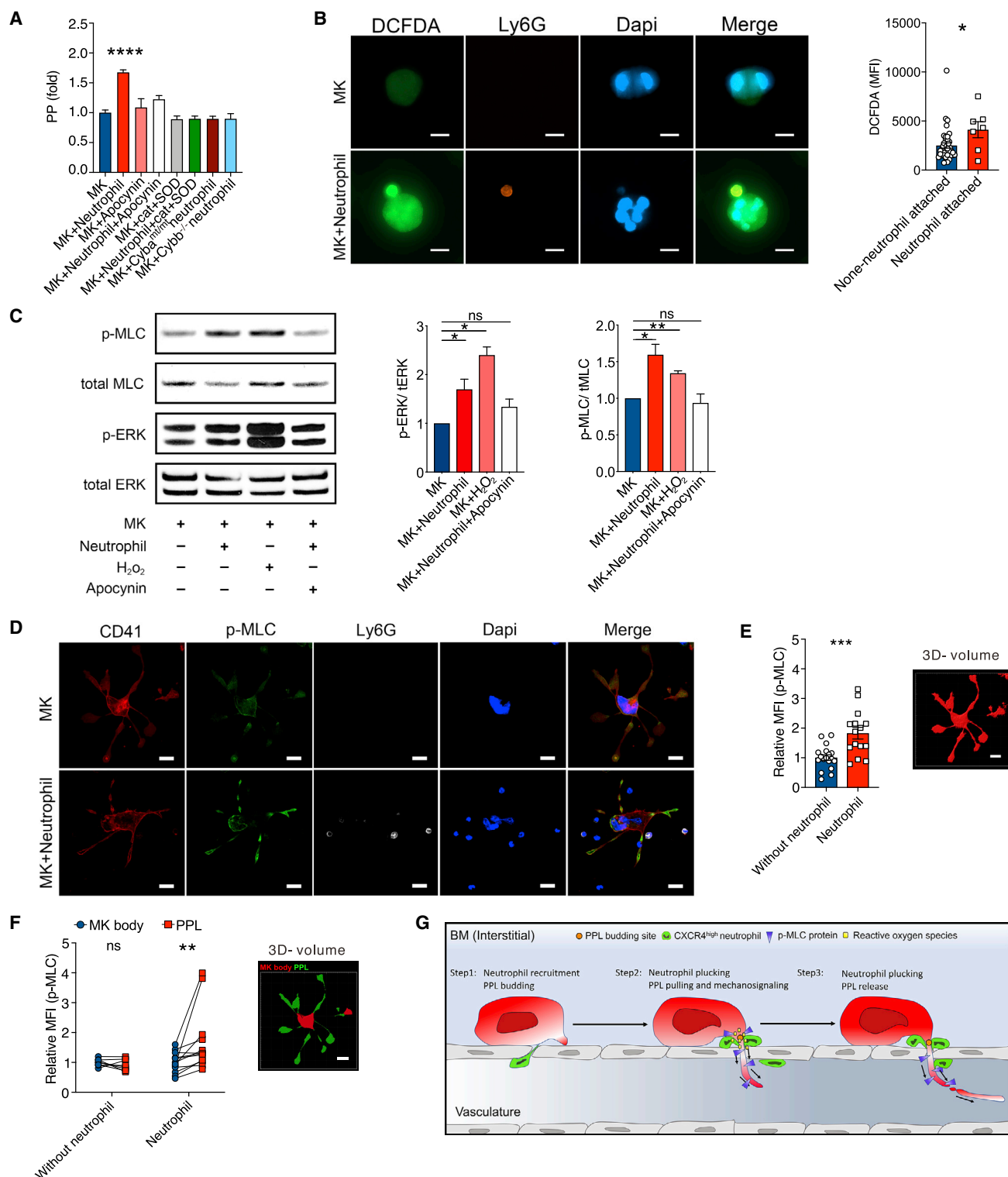
Figure 4. Neutrophil-derived reactive oxygen species drive thrombopoiesis

(A) PP release from *in vitro* MK cultures following co-culture with neutrophils in the presence or absence of NADPH inhibitor apocynin, superoxide dismutase (SOD) (50 U/ml), and catalase (50 μg/ml; n = 3), $Cyba^{mt/mt}$ or $Cybb^{-/-}$ neutrophils (n = 4 per group).

(B) Visualization of ROS in co-cultured MKs. ROS (DCFDA, green) mean fluorescent intensity in MKs with or without neutrophil interactions (Ly6G positive) was quantified. Symbols indicate individual MKs. Representative images of 3 independent experiments are shown, scale bar represents 10 μm.

were all increased following MI compared to control mice (Figures S5E and S5F). Abrogation of neutrophil CXCR4 signaling corrected disproportionate platelet production (i.e. platelets: −35.8%; reticulated platelets: −49.1%; vs. sham treatment) and normalized distant thrombus formation in *Mrp8-cre(+)/Cxcr4*$^{\Delta/\Delta}$ mice with a previous MI compared to controls without MI (Figures 6D, 6E, S5G–S5I, and Video S2). Thus, neutrophils underly the increased supply of immature platelets in the course of MI, in turn generating a prothrombotic milieu favoring repeat arterial thrombotic events.

Patients with a recent MI carry an increased risk of VTE after the initial thrombotic event (Khan et al., 2021; Rinde et al., 2016). To determine whether the prothrombotic effect of neutrophil-driven thrombopoiesis is a general mechanism driving thrombotic endpoints, we defined its role for VTE. Induction of deep venous thrombosis (DVT) in a vena cava thrombosis model in mice (von Bruhl et al., 2012) resulted in increased reticulated platelet counts (i.e. platelets: +22.6; reticulated platelets: +50.2%; vs. sham treatment; Figure S6A). In parallel, mouse VTE led to increased neutrophil counts, CXCR4 expression, and neutrophil tropism in BM resident MKs following adoptive transfer of neutrophils into DVT-treated animals (Figures S6B–S6D). When we exposed *Mrp8-cre Cxcr4*$^{fl/fl}$ mice to VTE, the number of prothrombogenic reticulated platelets was reduced (i.e. platelets: −28.2%; reticulated platelets: −44.3%; vs. sham treatment) (Figure S6E). At the same time, ablation of neutrophil CXCR4 resulted in reduced thrombus weights, while thrombus frequency (Figures 6F and 6G) and thrombus composition quantified by neutrophil, monocyte, and neutrophil-extracellular-trap (NET) densities (Figures S6F and S6G) were similar. Elevated reticulated platelet counts, arising from exacerbated neutrophil-driven thrombopoiesis, therefore foster thrombo-ischemic endpoints in two prototype thromboinflammatory cardiovascular diseases.

To test whether neutrophil plucking also controls platelet production in infection, we applied a model of lipopolysaccharide (LPS)-induced systemic inflammation. As expected, intraperitoneal LPS injection produced a rapid drop in platelet counts, followed by a prolonged platelet count recovery phase (Aslam et al., 2006). After 36 h, total platelet counts were still reduced in LPS-treated mice, while reticulated platelet counts were increased (Figure S7A) compared to control treatment. MK numbers remained unchanged (Figures S7B and S7C). We found increased neutrophil CXCR4 surface expression and ROS production after LPS treatment (Figures S7D and S7E), and *in vivo* imaging revealed increased MK-neutrophil interactions within the perisinusoidal space and accelerated PPL formation (Figures S7F–S7H). Ablation of neutrophil plucking in *Mrp8-cre(+)/Cxcr4*$^{\Delta/\Delta}$ mice decreased perisinusoidal MK-neutrophil

interactions, attenuated PPL formation kinetics, and delayed platelet count recovery 36 h after LPS treatment (Figure S7I–S7L).

DISCUSSION

Our study has identified a so far unexplored function of neutrophils that links sterile inflammation to platelet homeostasis and thrombosis. We have shown that neutrophils control thrombopoiesis by plucking on forming PPLs, in turn accelerating their growth and release into the circulation.

Inflammatory diseases are known to impact thrombopoiesis, yet the mechanisms behind this observation remain unknown. Different mechanisms including cytokine gradients (Lane et al., 2000; Zhang et al., 2012), changes in local vasculature (Stegner et al., 2017) and extracellular matrix composition (Stegner et al., 2017), sympathetic innervation (Chen et al., 2016), and shear forces (Junt et al., 2007) are involved in the control of megakaryo- and thrombopoiesis. Most of these pathways control platelet homeostasis in the long term but do not allow the rapid responses required for fine-tuning of platelet homeostasis and to provide immediate platelet supply in scenarios of increased platelet consumption. Here, we show that neutrophils are recruited to the PPL budding site of MKs via CXCR4-CXCL12 and control the last step of BM thrombopoiesis, i.e. release of PPLs by direct physical interaction. Plucking neutrophils accelerate PPL growth and release by induction of mechanosignaling in megakaryocytes through NOX2-dependent ROS (Figures 4A, 4C–4F, and S4). We propose that these mechanisms endow neutrophils with the ability to rapidly impact platelet homeostasis upon positioning around the PPL budding site. Thus, neutrophils outpace classical systemic feedback loops regulating platelet counts (i.e. cytokines) that partially depend on translational activity, posttranslational protein processing, and systemic distribution (Grozovsky et al., 2015; Nishimura et al., 2015; Burzynski et al., 2019).

We have shown here that plucking neutrophils are a rheostat of platelet homeostasis that maintain platelet counts under steady state but also boost release of immature platelets during thromboinflammation, thereby increasing the risk of arterial thrombosis and repeated ischemic events following MI. Previous data and our current findings suggest that immature platelets contribute to the increased risk of recurrent ischemia (Lakkis et al., 2004) and mortality (Cesari et al., 2013) in patients with MI. How immature platelets foster thrombotic processes remains to be defined, yet several mechanisms are likely to operate. Firstly, we demonstrated that immature platelets were preferentially recruited to sites of vascular damage after MI and are found more abundantly in arterial thrombi. Secondly, immature platelets showed a more activated phenotype,

(C) Representative immunoblots of 3 independent experiments from co-cultured MKs for p-MLC or p-ERK following the indicated treatment are shown. Phospho-signals were quantified and normalized to total MLC and ERK protein (n = 3).

(D) MK-neutrophil *in vitro* co-culture in the presence or absence of neutrophils. Immunofluorescence staining for p-MLC (green), CD41 (red; MKs), Ly6G (white; neutrophil), and DAPI (blue; nuclei). Representative confocal microscopy images of 4 independent experiments are shown (n = 4).

(E) Relative (compared to MK w/o neutrophil condition) single-cell p-MLC signal mean fluorescent intensity (MFI) following 3D reconstruction (symbols represent individual MKs). Scheme for p-MLC signal distribution analysis using 3D rendering technique to quantify MFI within the MK body versus PPL.

(F) p-MLC distribution within MKs that were cultured in the presence or absence of neutrophils is shown (symbols indicate individual MKs).

(G) Scheme of PPL-plucking mechanism by neutrophils during thrombopoiesis. Bars represent mean ± SEM; p values are indicated, *<0.05, **<0.01, ***<0.001, ****<0.0001, n.s. not significant. P values were determined using unpaired (B and E) or paired (F) Student's t test, (C) one-sided t test, and one-way (A) ANOVA multigroup test. Please see also Table S1 and Figure S4.
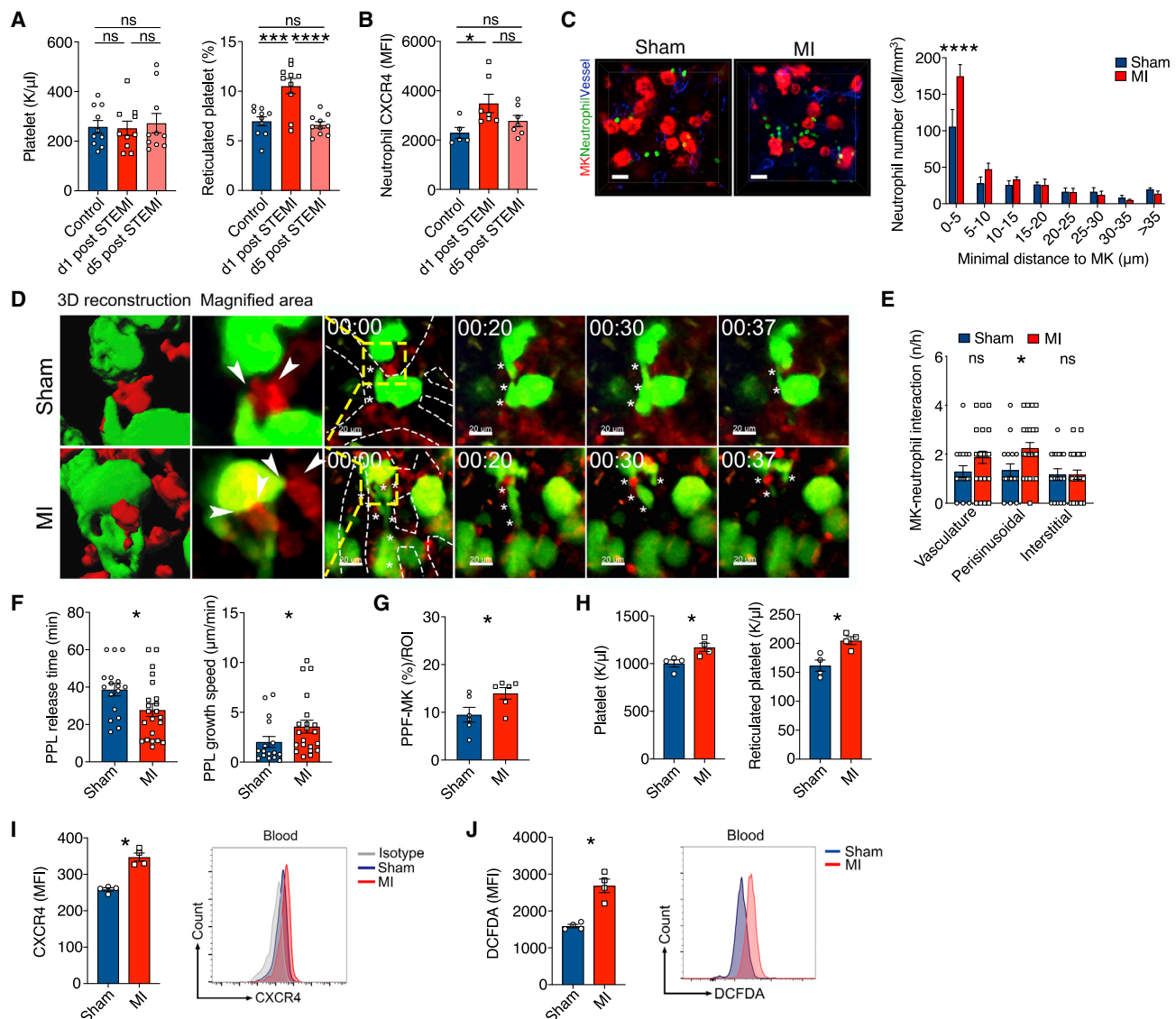
Figure 5. Myocardial infarction triggers thrombopoiesis by neutrophil plucking

(A and B) Patients admitted because of acute ST-elevation myocardial infarction (STEMI) with symptom onset <12 h undergoing revascularization by percutaneous coronary intervention or control patients with stable coronary artery disease were recruited. (A) Platelet counts and reticulated platelet fraction (control patients: n = 10; STEMI patients: n = 10, symbols indicate individual patients) and (B) neutrophil-expressed CXCR4 was determined by flow cytometry (control patients: n = 5; STEMI patients: n = 7, symbols indicate individual patients).

(C) Adoptive transfer experiments of neutrophils into I/R or sham-treated C57BL/6 mice. Representative 2D pictures from 3 independent experiments of whole-mount-stained bones are shown (scale bar represent 10 μm). Minimal MK-neutrophil distance between MKs and neutrophils was quantified (n = 3 animals per group).

(D–G) *In vivo* multiphoton visualization of MK-neutrophil interactions 48 h after I/R or sham treatment in C57BL/6 mice.

(D) Image series of PPL release in I/R and sham-treated mice is shown. Scale bars represent 20 μm (n = 3 animals per group), timeline (min) is indicated.

(E) Quantification of MK-neutrophil interaction frequencies within different compartments (n = 3 animals per group).

(F) Analysis of PPL growth speed and release time (n = 3 animals per group, each symbol indicates individual PPLs).

(G) Frequency of PPL-forming MKs (n = 3 animals per group, each symbol indicates individual ROI area).

(H) Platelet and reticulated platelet counts.

(I) CXCR4 surface expression on peripheral neutrophils was determined in I/R and sham-treated animals by flow cytometry (n = 4 animals per group), a representative histogram blot of 4 independent experiments is shown.

(J) Reactive oxygen species in peripheral neutrophils in I/R and sham-treated animals (n = 4 animals). Bars represent mean ± SEM, symbols indicate individual animals or MKs or ROIs; p values are indicated, *<0.05, ***<0.01, ****<0.0001, n.s. not significant. P values were determined by unpaired Student's t test (F, G, H, I, and J) or one-way (A and B) or two-way (C and E) ANOVA multigroup test. Please see also Table S2 and Figure S5.
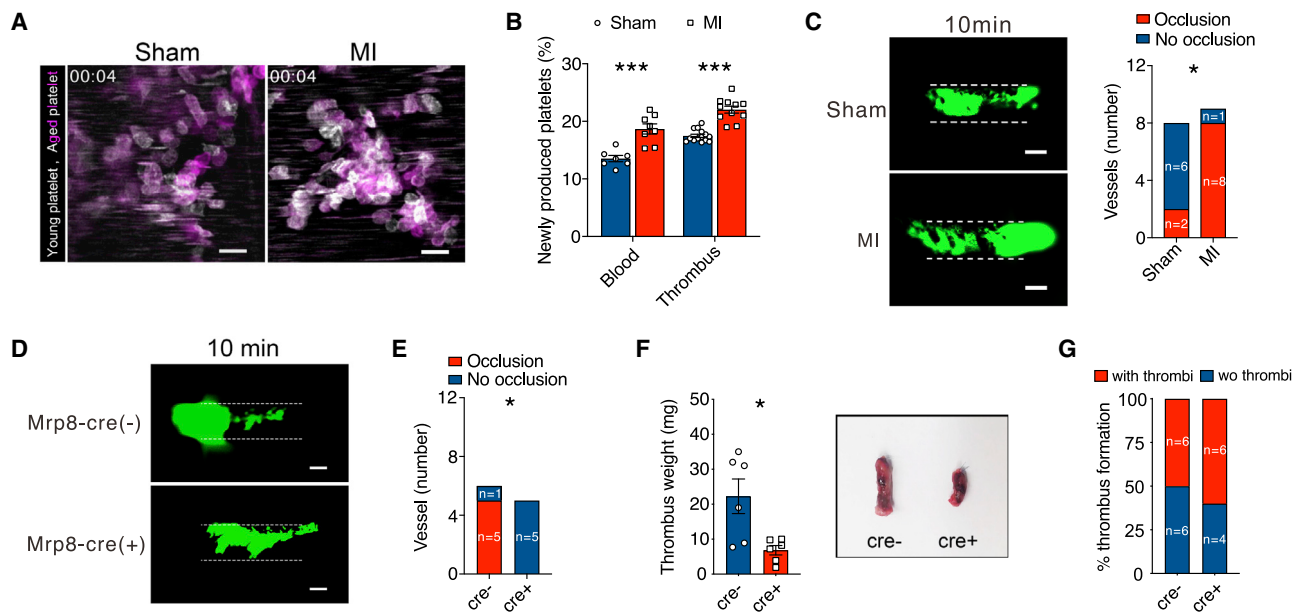
Figure 6. Genetic ablation of neutrophil CXCR4 prevents secondary ischemic events and reduces thrombus burden in cardiovascular diseases

(A and B) Fe-(III) chloride, mesenteric artery thrombosis in I/R and sham-treated animals. (A) Representative images of 7 (sham) or 8 (MI) independent experiments of platelet recruitment into forming thrombus are shown (scale bar represents 5 μm).

(B) Quantification of reticulated platelet fraction within peripheral blood and forming thrombus (sham: n = 7 animals; MI: n = 8 animals; multiple thrombi per mouse were quantified).

(C) Fe-(III) chloride induced carotid artery thrombosis in I/R and sham treated animals. Representative images of 8 (sham) or 9 (MI) independent experiments of formed thrombus are shown, dashed lines indicate vessel wall (scale bars represent 200 μm). Occlusive thrombus formation was analyzed (sham: n = 8 animals; MI: n = 9 animals).

(D) Fe-(III) chloride-induced carotid artery thrombosis in $Mrp8$-cre/cxcr4$^{fl/fl}$ mice 48 h after I/R and sham treatment. A representative image of formed thrombus is shown, dashed lines indicate vessel wall (scale bars represent 200 μm).

(E) Occlusive thrombus formation was analyzed by video analysis ($Mrp8$-cre[−]/cxcr4$^{fl/fl}$ n = 6 animals; ($Mrp8$-cre[+]/cxcr4$^{Δ/Δ}$ n = 5 animals).

(F) Vena cava thrombosis was induced in $Mrp8$-cre/cxcr4$^{fl/fl}$ mice. Thrombus weights were determined 48 h after induction of venous thrombosis, representative images of 3 independent experiments are shown.

(G) Thrombus frequency is shown. Bars represent mean ± SEM, symbols indicate individual animals; p values are indicated, *<0.05, ***<0.001, n.s. not significant. P values were determined with unpaired Student's t test (B and F) or Chi-square t test (C, E, and G). Please see also Figures S5 and S6.

facilitating platelet aggregation and driving coagulation at injury sites. Finally, immature platelets appeared to be less sensitive to current antiplatelet therapies (Bernlochner et al., 2015; Armstrong et al., 2017). Thus, targeting neutrophil-driven thrombopoiesis to attenuate supply of prothrombotic immature platelets may be an antithrombotic and antiischemic approach to prevent recurrent ischemia during the early phase of MI and other thromboinflammatory processes, including VTE. In summary, we have identified neutrophil-driven thrombopoiesis as a hallmark of common thrombotic cardiovascular diseases, highlighting its potential as a so far unexplored antithrombotic target.

Limitations of the study
Our study has some limitations arising from technical challenges in investigating cell-cell interactions within the bone marrow using life cell imaging. Mechanistically, we cannot dissect the contribution of neutrophil-transduced direct physical forces from neutrophil-induced mechanosignaling in MKs *in vivo*. While intracellular tension and force measurement using fluorescent probes are feasible, it is beyond the current state of the art to apply this approach on neutrophils within the bone marrow. Another limitation of our study is that we cannot directly prove

the presence of neutrophil plucking in human bone marrow. However, our human data revealed similar changes within the peripheral platelet and immune cell populations as seen in mice with MK plucking neutrophils.

STAR★METHODS

Detailed methods are provided in the online version of this paper and include the following:

- ● KEY RESOURCES TABLE
- ● RESOURCE AVAILABILITY
  - ○ Lead contact
  - ○ Materials availability
  - ○ Data and code availability
- ● EXPERIMENTAL MODEL AND SUBJECT DETAILS
  - ○ Mouse strains
- ● METHODS
  - ○ Primary-fetal-liver-cell-derived megakaryocyte culture
  - ○ BM-derived MK isolation
  - ○ Leukocyte isolation
  - ○ Co-culture

- ○ Co-culture (immunoblot)
- ○ Blood count analysis
- ○ Flow cytometry
- ○ Quantification of reticulated platelets
- ○ Neutrophil depletion
- ○ Monocyte and B cell depletion
- ○ N-acetylcysteine (NAC) treatment *in vivo*
- ○ Platelet lifespan measurement
- ○ Cell labeling for *in vivo* visualization
- ○ Intravital multiphoton imaging
- ○ Time lapse imaging of MK-neutrophil interactions *in vitro*
- ○ Adoptive neutrophil transfer
- ○ Adoptive neutrophil transfer in *Mrp8-cre*(+)/iDTR mice
- ○ Bone whole-mount staining
- ○ Immunofluorescent staining
- ○ ROS quantification
- ○ ROS visualization *in vitro*
- ○ Murine BM cytokine profile analysis
- ○ Acute myocardial infarction mouse model
- ○ Ferric(III) chloride-induced thrombus formation in the murine carotid artery model
- ○ Platelet recruitment into Fe(III) chloride-induced mesenteric artery thrombosis
- ○ Venous thrombosis model by flow restriction in the vena cava inferior
- ○ LPS model
- ○ Generation of bone marrow chimera
- ○ Human samples
- ● QUANTIFICATION AND STATISTICAL ANALYSIS
  - ○ GWAS analysis

SUPPLEMENTAL INFORMATION

Supplemental information can be found online at https://doi.org/10.1016/j.immuni.2022.10.001.

DECLARATION OF INTERESTS

The authors declare no competing interests.

INCLUSION AND DIVERSITY

We support inclusive, diverse, and equitable conduct of research.

REFERENCES

Adrover, J.M., Del Fresno, C., Crainiciuc, G., Cuartero, M.I., Casanova-Acebes, M., Weiss, L.A., Huerga-Encabo, H., Silvestre-Roig, C., Rossaint, J., Cossio, I., et al. (2019). A neutrophil timer coordinates immune defense and vascular protection. Immunity *51*, 966–967.

Armstrong, P.C., Hoefer, T., Knowles, R.B., Tucker, A.T., Hayman, M.A., Ferreira, P.M., Chan, M.V., and Warner, T.D. (2017). Newly formed reticulated platelets undermine pharmacokinetically short-lived antiplatelet therapies. Arterioscler. Thromb. Vasc. Biol. *37*, 949–956.

Aslam, R., Speck, E.R., Kim, M., Crow, A.R., Bang, K.W.A., Nestel, F.P., Ni, H., Lazarus, A.H., Freedman, J., and Semple, J.W. (2006). Platelet Toll-like receptor expression modulates lipopolysaccharide-induced thrombocytopenia and tumor necrosis factor-alpha production *in vivo*. Blood *107*, 637–641.

Bernlochner, I., Goedel, A., Plischke, C., Schüpke, S., Haller, B., Schulz, C., Mayer, K., Morath, T., Braun, S., Schunkert, H., et al. (2015). Impact of immature platelets on platelet response to ticagrelor and prasugrel in patients with acute coronary syndrome. Eur. Heart J. *36*, 3202–3210.

Boisset, J.C., Vivié, J., Grün, D., Muraro, M.J., Lyubimova, A., and Van Oudenaarden, A. (2018). Mapping the physical network of cellular interactions. Nat. Methods *15*, 547–553.

Bongiovanni, D., Santamaria, G., Klug, M., Santovito, D., Felicetta, A., Hristov, M., Von Scheidt, M., Aslani, M., Cibella, J., Weber, C., et al. (2019). Transcriptome analysis of reticulated platelets reveals a prothrombotic profile. Thromb. Haemost. *119*, 1795–1806.

Buch, T., Heppner, F., Tertilt, C., Heinen, T.J.A.J., Kremer, M., Wunderlich, F.T., Jung, S., and Waisman, A. (2005). A Cre-inducible diphtheria toxin receptor mediates cell lineage ablation after toxin administration. Nat Methods *2*, 419–426. https://doi.org/10.1038/nmeth762.

Burzynski, L.C., Humphry, M., Pyrillou, K., Wiggins, K.A., Chan, J.N.E., Figg, N., Kitt, L.L., Summers, C., Tatham, K.C., Martin, P.B., et al. (2019). The coagulation and immune systems are directly linked through the activation of Interleukin-1alpha by Thrombin. Immunity *50*, 1033–1042.e6.

Casanova-Acebes, M., Nicolás-Ávila, J.A., Li, J.L., García-Silva, S., Balachander, A., Rubio-Ponce, A., Weiss, L.A., Adrover, J.M., Burrows, K., A-González, N., et al. (2018). Neutrophils instruct homeostatic and pathological states in naive tissues. J. Exp. Med. *215*, 2778–2795.

Casanova-Acebes, M., Pitaval, C., Weiss, L.A., Nombela-Arrieta, C., Chèvre, R., A-González, N., Kunisaki, Y., Zhang, D., Van Rooijen, N., Silberstein, L.E., et al. (2013). Rhythmic modulation of the hematopoietic niche through neutrophil clearance. Cell *153*, 1025–1035.

Cesari, F., Marcucci, R., Gori, A.M., Caporale, R., Fanelli, A., Casola, G., Balzi, D., Barchielli, A., Valente, S., Giglioli, C., et al. (2013). Reticulated platelets

predict cardiovascular death in acute coronary syndrome patients. Insights from the AMI-Florence 2 Study. Thromb. Haemost. 109, 846–853.

Chang, Y., Auradé, F., Larbret, F., Zhang, Y., Le Couedic, J.P., Momeux, L., Larghero, J., Bertoglio, J., Louache, F., Cramer, E., et al. (2007). Proplatelet formation is regulated by the Rho/ROCK pathway. Blood 109, 4229–4236.

Chen, S., Du, C., Shen, M., Zhao, G., Xu, Y., Yang, K., Wang, X., Li, F., Zeng, D., Chen, F., et al. (2016). Sympathetic stimulation facilitates thrombopoiesis by promoting megakaryocyte adhesion, migration, and proplatelet formation. Blood 127, 1024–1035.

Cunin, P., Bouslama, R., Machlus, K.R., Martínez-Bonet, M., Lee, P.Y., Wactor, A., Nelson-Maney, N., Morris, A., Guo, L., Weyrich, A., et al. (2019). Megakaryocyte emperipolesis mediates membrane transfer from intracytoplasmic neutrophils to platelets. Elife 8, e44031.

Demircik, F., Buch, T., and Waisman, A. (2013). Efficient B cell depletion via diphtheria toxin in CD19-Cre/iDTR mice. PLoS One 8, e60643.

Faust, N., Varas, F., Kelly, L.M., Heck, S., and Graf, T. (2000). Insertion of enhanced green fluorescent protein into the lysozyme gene creates mice with green fluorescent granulocytes and macrophages. Blood 96, 719–726. https://doi.org/10.1182/blood.V96.2.719.

Greenbaum, A., Hsu, Y.-M.S., Day, R.B., Schuettpelz, L.G., Christopher, M.J., Borgerding, J.N., Nagasawa, T., and Link, D.C. (2013). CXCL12 in early mesenchymal progenitors is required for haematopoietic stem-cell maintenance. Nature 495, 227–230. https://doi.org/10.1038/nature 11926.

Grozovsky, R., Begonja, A.J., Liu, K., Visner, G., Hartwig, J.H., Falet, H., and Hoffmeister, K.M. (2015). The Ashwell-Morell receptor regulates hepatic thrombopoietin production via JAK2-STAT3 signaling. Nat. Med. 21, 47–54.

Hasenberg, A., Hasenberg, M., Männ, L., Neumann, F., Borkenstein, L., Stecher, M., Kraus, A., Engel, D.R., Klingberg, A., Seddigh, P., et al. (2015). Catchup: a mouse model for imaging-based tracking and modulation of neutrophil granulocytes. Nat. Methods 12, 445–452.

Itkin, T., Gur-Cohen, S., Spencer, J.A., Schajnovitz, A., Ramasamy, S.K., Kusumbe, A.P., Ledergor, G., Jung, Y., Milo, I., Poulos, M.G., et al. (2016). Distinct bone marrow blood vessels differentially regulate haematopoiesis. Nature 532, 323–328.

Junt, T., Schulze, H., Chen, Z., Massberg, S., Goerge, T., Krueger, A., Wagner, D.D., Graf, T., Italiano, J.E., Jr., Shivdasani, R.A., and Von Andrian, U.H. (2007). Dynamic visualization of thrombopoiesis within bone marrow. Science 317, 1767–1770.

Khan, F., Tritschler, T., Kahn, S.R., and Rodger, M.A. (2021). Venous thromboembolism. Lancet 398, 64–77.

Lakkis, N., Dokainish, H., Abuzahra, M., Tsyboulev, V., Jorgensen, J., De Leon, A.P., and Saleem, A. (2004). Reticulated platelets in acute coronary syndrome: a marker of platelet activity. J. Am. Coll. Cardiol. 44, 2091–2093.

Lane, W.J., Dias, S., Hattori, K., Heissig, B., Choy, M., Rabbany, S.Y., Wood, J., Moore, M.A., and Rafii, S. (2000). Stromal-derived factor 1-induced megakaryocyte migration and platelet production is dependent on matrix metalloproteinases. Blood 96, 4152–4159.

Livet, J., Weissman, T.A., Kang, H., Draft, R.W., Lu, J., Bennis, R.A., Sanes, J.R., and Lichtman, J.W. (2007). Transgenic strategies for combinatorial expression of fluorescent proteins in the nervous system. Nature 450, 56–62. https://doi.org/10.1038/nature06293.

Machlus, K.R., and Italiano, J.E., JR. (2013). The incredible journey: From megakaryocyte development to platelet formation. J. Cell Biol. 201, 785–796.

Mack, M., Cihak, J., Simonis, C., Luckow, B., Proudfoot, A.E., Plachý, J., Brühl, H., Frink, M., Anders, H.J., Vielhauer, V., et al. (2001). Expression and characterization of the chemokine receptors CCR2 and CCR5 in mice. J. Immunol. 166, 4697–4704.

Massberg, S., Konrad, I., Schürzinger, K., Lorenz, M., Schneider, S., Zohlnhoefer, D., Hoppe, K., Schiemann, M., Kennerknecht, E., Sauer, S., et al. (2006). Platelets secrete stromal cell-derived factor 1alpha and recruit bone marrow-derived progenitor cells to arterial thrombi in vivo. J. Exp. Med. 203, 1221–1233.

Mazharian, A., Watson, S.P., and Séverin, S. (2009). Critical role for ERK1/2 in bone marrow and fetal liver-derived primary megakaryocyte differentiation, motility, and proplatelet formation. Exp. Hematol. 37, 1238–1249.e5.

Mccrann, D.J., Eliades, A., Makitalo, M., Matsuno, K., and Ravid, K. (2009). Differential expression of NADPH oxidases in megakaryocytes and their role in polyploidy. Blood 114, 1243–1249.

Mombaerts, P., Iacomini, J., Johnson, R.S., Herrup, K., Tonegawa, S., and Papaioannou, V.E. (1992). RAG-1-deficient mice have no mature B and T lymphocytes. Cell 68, 869–877.

Nakano, Y., Longo-Guess, C.M., Bergstrom, D.E., Nauseef, W.M., Jones, S.M., and Bánfi, B. (2008). Mutation of the Cyba gene encoding p22phox causes vestibular and immune defects in mice. J. Clin. Invest. 118, 1176–1185.

Nie, Y., Waite, J., Brewer, F., Sunshine, M.-J., Littman, D.R., and Zou, Y.-R. (2004). The Role of CXCR4 in Maintaining Peripheral B Cell Compartments and Humoral Immunity. J Exp Med 200, 1145–1156. https://doi.org/10.1084/jem.20041185.

Nishimura, S., Nagasaki, M., Kunishima, S., Sawaguchi, A., Sakata, A., Sakaguchi, H., Ohmori, T., Manabe, I., Italiano, J.E., Jr., Ryu, T., et al. (2015). IL-1alpha induces thrombopoiesis through megakaryocyte rupture in response to acute platelet needs. J. Cell Biol. 209, 453–466.

Noetzli, L.J., French, S.L., and Machlus, K.R. (2019). New insights into the differentiation of Megakaryocytes from Hematopoietic Progenitors. Arterioscler. Thromb. Vasc. Biol. 39, 1288–1300.

Passegué, E., Wagner, E.F., and Weissman, I.L. (2004). JunB Deficiency Leads to a Myeloproliferative Disorder Arising from Hematopoietic Stem Cells. Cell 119, 431–443. https://doi.org/10.1016/j.cell.2004.10.010.

Petzold, T., Ruppert, R., Pandey, D., Barocke, V., Meyer, H., Lorenz, M., Zhang, L., Siess, W., Massberg, S., and Moser, M. (2013). beta1 integrin-mediated signals are required for platelet granule secretion and hemostasis in mouse. Blood 122, 2723–2731.

Pollock, J.D., Williams, D.A., Gifford, M.A., Li, L.L., Du, X., Fisherman, J., Orkin, S.H., Doerschuk, C.M., and Dinauer, M.C. (1995). Mouse model of X-linked chronic granulomatous disease, an inherited defect in phagocyte superoxide production. Nat. Genet. 9, 202–209.

Rinde, L.B., Lind, C., Småbrekke, B., Njølstad, I., Mathiesen, E.B., Wilsgaard, T., Løchen, M.L., Hald, E.M., Vik, A., Braekkan, S.K., and Hansen, J.B. (2016). Impact of incident myocardial infarction on the risk of venous thromboembolism: the Tromso Study. J. Thromb. Haemost. 14, 1183–1191.

Sommers, C.L., Dejarnette, J.B., Huang, K., Lee, J., El-Khoury, D., Shores, E.W., and Love, P.E. (2000). Function of CD3 epsilon-mediated signals in T cell development. J. Exp. Med. 192, 913–919.

Stark, K., and Massberg, S. (2021). Interplay between inflammation and thrombosis in cardiovascular pathology. Nat. Rev. Cardiol. 18, 666–682.

Stegner, D., Vaneeuwijk, J.M.M., Angay, O., Gorelashvili, M.G., Semeniak, D., Pinnecker, J., Schmithausen, P., Meyer, I., Friedrich, M., Dütting, S., et al. (2017). Thrombopoiesis is spatially regulated by the bone marrow vasculature. Nat. Commun. 8, 127.

Tiedt, R., Schomber, T., Hao-Shen, H., and Skoda, R.C. (2007). Pf4-Cre transgenic mice allow the generation of lineage-restricted gene knockouts for studying megakaryocyte and platelet function in vivo. Blood 109, 1503–1506. https://doi.org/10.1182/blood-2006-04-020362.

von Brühl, M.L., Stark, K., Steinhart, A., Chandraratne, S., Konrad, I., Lorenz, M., Khandoga, A., Tirniceriu, A., Coletti, R., Köllnberger, M., et al. (2012). Monocytes, neutrophils, and platelets cooperate to initiate and propagate venous thrombosis in mice in vivo. J. Exp. Med. 209, 819–835.

Vuckovic, D., Bao, E.L., Akbari, P., Lareau, C.A., Mousas, A., Jiang, T., Chen, M.H., Raffield, L.M., Tardaguila, M., Huffman, J.E., Ritchie, S.C., et al. (2020). The polygenic and monogenic basis of blood traits and diseases. Cell 182, 1214–1231.e11.

Xia, L., Sperandio, M., Yago, T., Mcdaniel, J.M., Cummings, R.D., Pearson-White, S., Ley, K., and Mcever, R.P. (2002). P-selectin glycoprotein ligand-1-deficient mice have impaired leukocyte tethering to E-selectin under flow. J. Clin. Invest. *109*, 939–950.

Yang, J., Hirata, T., Croce, K., Merrill-Skoloff, G., Tchernychev, B., Williams, E., Flaumenhaft, R., Furie, B.C., and Furie, B. (1999). Targeted gene disruption demonstrates that P-selectin glycoprotein ligand 1 (PSGL-1) is required for

P-selectin-mediated but not E-selectin-mediated neutrophil rolling and migration. J. Exp. Med. *190*, 1769–1782.

Zhang, L., Orban, M., Lorenz, M., Barocke, V., Braun, D., Urtz, N., Schulz, C., von Brühl, M.L., Tirniceriu, A., Gaertner, F., et al. (2012). A novel role of sphingosine 1-phosphate receptor S1pr1 in mouse thrombopoiesis. J. Exp. Med. *209*, 2165–2181.

STAR★METHODS

KEY RESOURCES TABLE

REAGENT or RESOURCE	SOURCE	IDENTIFIER
Antibodies		
Ultra-LEAF Purified anti-mouse Ly-6G/Ly-6C (clone RB6-8C5), neutrophil depletion	Biolegend	Cat#108453; RRID:AB_2616681
Ultra-LEAF™ Purified Rat IgG2b, κ Isotype Ctrl (clone RTK4530)	Biolegend	Cat# 400671; RRID:AB_11147763
Pacific Blue™ anti-mouse Ly-6G/Ly-6C (clone RB6-8C5)	Biolegend	Cat#108430; RRID: AB_893556
PE anti-mouse CD115 (clone AFS98)	Biolegend	Cat#135506; RRID: AB_1937253
PE anti-mouse Ly-6G antibody (clone 1A8)	Biolegend	Cat#127608; RRID: AB_1186099
APC anti-mouse/rat CD42d (clone 1C2)	Biolegend	Cat#148506; RRID: AB_2564602
Pacific Blue™ anti-mouse Ly-6G Antibody	Biolegend	Cat#127612; RRID: AB_2251161
PerCP/Cyanine5.5 anti-mouse CD154 Antibody	Biolegend	Cat#106514; RRID: AB_2563498
APC/Cyanine7 anti-mouse CD63 Antibody	Biolegend	Cat#143908; RRID: AB_2565498
Pacific Blue™ anti-mouse/rat CD29 Antibody	Biolegend	Cat#102224; RRID: AB_2128079
FITC anti-mouse CD3 complex (clone 17A2)	BD Bioscience	Cat#555274; RRID: AB_395698
FITC anti-mouse CD61 (clone 2C9.G2)	BD Bioscience	Cat#553346; RRID: AB_10895806
BV711 Rat Anti-Mouse CD62P	BD Bioscience	Cat#740693; RRID: AB_2740377
PE-Cyanine5 anti Human/Mouse CD45R (clone RA3-6B2)	ebioscience	Cat#15–045282; RRID: AB 468755
FITC anti-mouse CD41a (clone MWReg30)	ebioscience	Cat#11-0411-85; RRID: AB_763483
Biotin anti-mouse CD41a (clone MWReg30)	ebioscience	Cat#13-0411-82; RRID: AB_763484
PE anti-mouse CXCR4 (clone 2B11)	ebioscience	Cat#12-9991-82; RRID: AB_891391
Streptavidin eFluor 450	ebioscience	Cat#48-4317-82,RRID:AB_10359737
Streptavidin PE	ebioscience	Cat#12-4317-87
Biotin anti-mouse VE-cadherin (clone eBioBV13)	ebioscience	Cat#13-1441-82; RRID: AB_1234997
GFP recombinant rabbit monoclonal antibody	Invitrogen	Cat#G10362; RRID: AB_2536526
Goat anti-Rat IgG (H + L) Cross-Adsorbed Secondary Antibody, Alexa Fluor 647	Invitrogen	Cat#A-21247; RRID:AB_141778
F(ab')2-Goat anti-Rabbit IgG (H + L) Cross-Adsorbed Secondary Antibody, Alexa Fluor 488	Invitrogen	Cat#A-11070; RRID: AB_2534114
DyLight 649 anti-mouse CD42b	emfret	Cat# M040-
Antibodies for *In Vivo* Mouse Platelet Labeling	emfret	Cat#X488; RRID: AB_2890921
Antibodies for *In Vivo* Mouse Platelet Labeling	emfret	Cat#X649; RRID: AB_2861336
Integrin alphaIIb beta3 (GPIIb/IIIa, CD41/CD61)	emfret	Cat#M023-2; RRID: AB_2833084
Rabbit Anti-Myeloperoxidase Polyclonal Antibody	Abcam	Cat#ab9535; RRID: AB_307322
Alexa 488 anti-mouse GPIX	p0p6-derivative Stegner lab	N/A
Mouse GPVI Alexa Fluor® 647-conjugated Antibody	R&D systems	Cat# FAB6758R
Human/Mouse CXCL12/SDF-1 Antibody	R&D systems	Cat#MAB350; RRID: AB_2088149
Phospho-p44/42 MAPK (Erk1/2) (Thr202/Tyr204) antibody	Cell Signaling	Cat#4370,RRID: AB_2315112
p44/42 MAPK (Erk1/2) (137F5) Rabbit mAb antibody	Cell Signaling	Cat#4695; RRID: AB_390779
Phospho-Myosin Light Chain 2 (Ser19) Antibody	Cell Signaling	Cat#3671; RRID: AB_330248
Myosin Light Chain 2 Antibody	Cell Signaling	Cat#3672; RRID: 10692513
Goat anti-Rabbit IgG (H + L) Secondary Antibody, HRP	Thermo scientific	Cat#31460; RRID: AB_228341
MC-21(anti-CCR2) antibody	Courtesy Matthias Mack	N/A

Continued

REAGENT or RESOURCE	SOURCE	IDENTIFIER
Experimental models: Organisms/strains		
C57BL/6J	Jackson Laboratory	N/A
Mrp8-cre	Passegué et al., 2004	B6.Cg-Tg(*S100A8-cre*,-EGFP)1Ilw
Rosa26-Confetti	Livet et al., 2007	Gt(ROSA)26Sor$^{tm1(CAG-Brainbow2.1)Cle}$/J
Rosa26-iDTR	Buch et al., 2005	C57BL/6-Gt(ROSA)26Sor$^{tm1(HBEGF)Awai}$/J
Lyz2-eGFP	Faust et al., 2000	B6.129P-*Lyz2*$^{tm1(EGFP)1.1Graf}$
Cxcl12 $^{fl/fl}$	Greenbaum et al., 2013	B6(FVB)-*Cxcl12*$^{tm1.1Link}$/J
Pf4-cre	Tiedt et al., 2007	C57BL/6-Tg(*Pf4*-icre)Q3Rsko/J
Cxcr4 $^{fl/fl}$	Nie et al., 2004	B6.129P2-*Cxcr4*^{tm2Yzo}/J
Selplg$^{-/-}$	Yang et al., 1999	B6.Cg-*Selplg*^{tm1Fur}/J
Catchup	Hasenberg et al., 2015	B6.Ly6g$^{tm1.1(cre)Gunz}$
Cyba$^{mt/mt}$	Nakano et al., 2008	A.B6 Tyr + -*Cyba*^{nmf333}/J
Cd19-cre	Demircik et al., 2013	B6.129P2(C)-Cd19$^{tm1(cre)Cgn}$/J
Cd3e$^{-/-}$	Sommers et al., 2000	B6; 129-Cd3e^{tm1Lov}/J
Rag1$^{-/-}$	Mombaerts et al., 1992	B6.129S7-*Rag1*^{tm1Mom}/J
Chemicals and recombinant proteins		
Thiazole Orange	Sigma-Aldrich	Cat# 390062
2′,7′-Dichlorodihydrofluorescein diacetate	Sigma-Aldrich	Cat# D6883
EZ-Link™ Sulfo-NHS-Biotin	Thermo Fisher	Cat# 27217
Phorbol 12-myristate 13-acetate	Sigma-Aldrich	Cat# P8139
Mouse recombinant thrombopoietin	Immunotools	Cat# 12343615
Mouse recombinant SDF-1 alpha	Immunotools	Cat# 12343365
Apocynin	Sigma-Aldrich	Cat# 10809
Qtracker705 Vascular labels	Thermo Fisher	Cat# Q21061MP
AMD3100	Tocris	Cat# 3299
U46619	Cayman	Cat#16450
Thrombin	Chrono-Log	Cat# P/N386
Proteome Profiler Mouse XL Cytokine Array	R&D systems	Cat# ARY028
ML-7 hydrochloride	MedChemExpress	Cat#HY-15417
FR180204	MedChemExpress	Cat# HY-12275
Critical commercial assays		
Neutrophil Isolation Kit, mouse	Miltenyi Biotec	Cat# 130-097-658
μ-Slide 4 Well	Ibidi	Cat# 80426
Pan T Cell Isolation Kit II, mouse	Miltenyi Biotec	Cat# 130-095-130
Monocyte Isolation Kit (BM), mouse	Miltenyi Biotec	Cat# 130-100-629
Pan B Cell Isolation Kit II, mouse	Miltenyi Biotec	Cat# 130-095-813
Software and algorithms		
Imaris	Bitplane	RRID:SCR_007370
Flowjo vX	Treestar	RRID:SCR_008520
Prism	Graphpad	RRID:SCR_002798
ImageJ	NIH	RRID:SCR_003070

RESOURCE AVAILABILITY

All data are available in the main text or the supplementary materials.

Lead contact
Further information and requests for resources and reagents should be directed to and will be fulfilled by the lead contact, Tobias Petzold (Tobias.Petzold@med.uni-muenchen.de).

Materials availability
This study did not generate new unique reagents. All reagents generated or used in this study are available on request from the lead contact with a completed Materials Transfer Agreement. Information on reagents used in this study is available in the key resources table.

Data and code availability
All the data supporting the findings of the article are available within the main text or supplementary materials.

EXPERIMENTAL MODEL AND SUBJECT DETAILS

Mouse strains
C57BL/6J, *Pf4-cre* (C57BL/6-Tg(*Pf4*-cre)Q3Rsko/J), Rosa26-Confetti (Gt(ROSA)26Sortm1(CAG-Brainbow2.1)Cle/J), *Lyz2*-eGFP (B6.129P-Lyz2tm1(EGFP)1.1Graf), *Cxcl12*$^{fl/fl}$(B6(FVB)-Cxcl12tm1.1Link/J), *Cybb* (B6.129S-Cybbtm1Din/J) mice were purchased from Jackson Laboratory and were kept under pathogen free conditions. Rag-1 deficient mice, *Mrp8-cre* mice (B6.Cg-Tg(S100A8-cre,-EGFP)1Ilw), *Cxcr4*$^{fl/fl}$ (B6.129P2-Cxcr4tm2Yzo/J) mice or Rosa26-iDTR (C57BL/6-Gt(ROSA26)Sortm1(HBEGF) Awai/J) mice were kindly provided by Prof. Andres Hidalgo and crossed to generate *Mrp8-cre*/cxcr4$^{fl/fl}$ and *Mrp8-cre*/Rosa26iDTR mice. Catchup mice (Hasenberg et al., 2015) were a gift from Prof. Matthias Gunzer. *Cyba*$^{mt/mt}$ (A.B6 Tyr + -Cybanmf333/J) mice were provided by Prof. Agnes Görlach. *Selplg*$^{-/-}$ deficient mice were kindly provided Prof. Vestweber (Xia et al., 2002). CD3e deficient mice (Sommers et al., 2000) were kindly supported by Prof. Marc Schmidt-Supprian. Mx1-Cre integrin *Itgb1*$^{fl/fl}$ and Kindlin-3$^{-/-}$ mice were kindly provided by Dr. Markus Moser. CD19-Cre/Rosa26iDTR mice were kindly provided by Dr. Wenyan He. To generate *Pf4-cre*(+)/ Confetti$^{-/-}$/*Lyz2*-eGFP mice, Rosa26-Confetti mice were crossed with *Pf4-cre* (and subsequently with *Lyz2*-eGFP mice. All mouse strains were backcrossed and maintained on a C57BL/6 background. If not otherwise indicated, mouse of same sex and age were paired and assigned into experimental groups. All experiments performed on mice were approved by Bavarian local legislation on animal protection.

METHODS

Primary-fetal-liver-cell-derived megakaryocyte culture
Murine fetal liver cells were harvested on embryonic day 13.5–14.5 as described before (Zhang et al., 2012). Suspended cells were cultured in DMEM medium (10% fetal bovine serum+1% penicillin/streptomycin) containing 70 ng/ml thrombopoietin (TPO, ImmunoTools) for 5 days at 37°C and 5%CO$_2$. On day five, megakaryocytes were enriched using a bovine serum albumin (BSA) gradient method.

BM-derived MK isolation
Femur and humerus bones were isolated and BM was flushed with 2% FCS/PBS. Cells were resuspended as single cell population to pass a 70 µm cell strainer. Cells were centrifuged, resuspended in DMEM medium and supplemented with 10% FBS and 1% penicillin/streptomycin. Cells were cultured in 6-well plates in DMEM medium with 10% FBS and 1% penicillin/streptomycin, 70 ng TPO and 15 U/ml heparin for 5 days at 37°C (5% CO$_2$). MKs were enriched using a BSA gradient (3%–1.5%–0% BSA in PBS) over 30 min twice.

Leukocyte isolation
Murine neutrophils were isolated from large bones by flushing the BM with PBS supplemented with 2% FCS. BM cells were resuspended with a 20-gauge syringe needle and filtered by 40 µm strainer, followed by centrifugation at 300 x g for 5 min at room temperature (RT). Erythrocyte lysis was performed by addition of lysis buffer (155 mM NH4Cl2, 10 mM KHCO3, 0.1 mM EDTA, pH 7.3). Lysis reaction was stopped after 5 min by addition of PBS containing 2 mM EDTA. Neutrophils were enriched using a murine neutrophil enrichment kit (Miltenyi Biotec) according to the manufacturer's instruction. B-cells, T-cells and monocytes were harvested from spleen (B-cells and T-cells) or BM. Murine spleen was cut and grinded into small pieces by scalpel and syringe. Then cells were resuspended into single cells suspension by 20-gauge syringe needle with 2% FCS/PBS. Afterward, B-cells and T-cells were isolated and enriched by isolation kit (Miltenyi Biotec) following the manufacturer's instructions. Monocytes were isolated in analogy to neutrophils. For monocyte isolation from the BM an murine monocyte isolation kit (Miltenyi Biotec) was used.

Co-culture
For co-culture assays 2.5 x 10^4 BM-derived megakaryocytes or fetal liver cells (FLC) (for stainings) were seeded in 6-wells dishes coated with 100 µg/ml fibrinogen and cultured in medium [40% (DMEM+10% fetal bovine serum+1% Penicillin/Streptomycin) with 60% Leibovitz L15 medium] for 6 hours at 37°C and 5%CO$_2$. After 30 min 2,5 x 10^5 neutrophils were added to the MK culture. MK-leukocyte ratios were adapted according to their neutrophil count ratio (100% neutrophils, 75% B-cells, 24% monocytes, 12% T-cells). If indicated, blocking antibody treatment was started immediately before co-culturing. If indicated, neutrophils were pre-incubated with cytochalasin D (100 nM) or blebbistatin (50 nM) for 30 min at 37°C before being added into the co-culture with MKs. After 6 h supernatants were collected and fixed with 1% paraformaldehyde (PFA) for 10 min at RT. Released platelet particles

(PP) were centrifuged and stained with directly fluorescently labelled antibodies for CD42d-APC, Ly6G-PE and CD61-FITC before being analyzed by flow cytometry.

Co-culture (immunoblot)

Co-culture experiments were performed as described above. MKs were incubated with 2.5×10^6 neutrophils in the presence of 30 nM apocynin or 30 nM H_2O_2 for 6 hours. To isolate a clean MK population, neutrophils were flushed away by repetitive washing steps with 1x cold Tris-buffered saline. Successful removal was confirmed by microscopy. Next, adherent megakaryocytes were scraped off before homogenized in cold RIPA buffer containing 50 nM protease and phosphatase inhibitors (Thermo Fischer). Samples (10 μg) were prepared and subjected to immunoblotting. Following the blot step, the PVDF membrane was incubated with the following antibodies: p-ERK, t-ERK, p-MLC and t-MLC. Thereafter, membranes were incubated with HRP coupled secondary antibody (1:5000 or 1:30000 respectively). Chemiluminescence signals were detected on X-ray film (Fuji) after addition of chemiluminescent detection reagent to the membrane (ECL, Merck). Relative signal strengths were determined by densitometry using ImageJ software.

Blood count analysis

Murine blood was drawn by intracardial puncture from anesthetized [isoflurane (DeltaSelect), fentanyl i.p. (0.05 mg/kg body weight; CuraMed Pharma)] mice and collected in a tube containing acid citrate dextrose (39 mM citric acid, 75 mM sodium citrate, 135 mM dextrose; ACD) buffer. Blood counts were analyzed on a hematology system blood counter (IDEXX ProCyte DX) or Gallios flow cytometer (Beckman) / BD FACSCantoII flow cytometer (BD) after addition of specific labelling antibodies (i.e. CD41) and fluorescent bead calibration. Therefore, 2 μL murine blood was stained with the respective antibody (dilution 1:100) for 20 min at RT in the dark before 4 μL multifluorescent counting beads were added and flow cytometry analysis was performed.

Flow cytometry

Erythrocyte-lysed whole blood or bone marrow cells were surface-stained in PBS for 30 min at 4°C. Multiparametric flow cytometric analyses were performed on Gallios flow cytometer (Beckman) or BD FACSCantoII flow cytometer (BD). Dead cells were excluded by FSC, SSC and 49,6-diamino-2-phenylin-dole (DAPI) stain. Neutrophils were gated as Gr-1$^+$ (RB6-8C5)/ CD115$^-$ (AFS98) events; monocytes, B-cells or T-cells were gated as Gr-1$^+$/ CD115$^+$, CD45R$^+$ (RA3-6B2) or CD3$^+$ (17A2) events respectively. Mature MKs were gated by as CD41$^+$/CD42d$^+$ double positive population. MK ploidy was quantified following propidium iodide staining in MKs.

Quantification of reticulated platelets

Reticulated platelet counts were determined by analyzing fixed (1% PFA for 10 min) citrate blood. Human reticulated platelets were stained with CD41-PE (1:100) and thiazole orange (250 ng/ml) for 20 min, before being analyzed by flow cytometry. Murine reticulated platelets were detected following a double staining with CD42d-PE antibody and thiazole orange (1 μg/ml).

Neutrophil depletion

For neutrophil depletion 50 μg Gr-1 antibody (RB6-8C5 clone) was injected by tail vein or 3 times every second day. For diphtheria toxin (DT)-induced neutrophil depletion, *Mrp8-cre*/Rosa26-iDTR mice received 10 ng/g body weight DT over 5 consecutive days by i.p. injection.

Monocyte and B cell depletion

To deplete monocytes *in vivo*, 10–12 weeks old, C57BL/6 male mice received (i.p.) 5 consecutive days anti-CCR2 (MC-21) or isotype control antibody, 20 μg/per mouse daily. For B-lymphocyte depletion, Cd19-*cre*/iDTR mice received (i.p.) 3 consecutive days diphtheria toxin, 10 ng/g body weight per day.

N-acetylcysteine (NAC) treatment *in vivo*

10–12 weeks old mice were assigned to receive 200 mg/kg body weight N-acetylcysteine or 0.9%NaCl (vehicle) i.p. over 5 days. At treatment day five mice were euthanized and blood and bones were harvested for further analysis.

Platelet lifespan measurement

To quantify platelet lifespan a biotin pulse labelling assay was performed. Therefore 30 mg/kg body weight Sulfo-NHS-biotin was injected i.v. At the indicated time points 20 μL blood was collected in ACD buffer after tail vein puncture. Whole blood was stained with 1:100 streptavidin-PE (SA-PE) to stain biotin labelled cells in addition to a CD42d-APC labelling to identify the total platelet fraction.

Cell labeling for *in vivo* visualization

To visualize neutrophils and MKs simultaneously *in vivo*, 5 μg Ly6G-PE antibody (Biolegend) or 15 μg anti-GPIX-Alexa488 derivative antibody was administered i.v.

Intravital multiphoton imaging

Preparation of the calvarium was performed as described before (*13*) (Zhang et al., 2012). Briefly 10–18 weeks old mice received anesthesia with 5.0 Vol. % isoflurane and 2% oxygen, followed by an i.p. injection of MMF solution (90 μL Midazolam (0.5 mg/kg), 15 μL Meditomidin (0.05 mg/kg) and 90 μL Fentanyl (5 mg/kg)) with repetitive injections every 45 min. A PE-10 polyethylene catheter was placed into the murine tail vein for fluids and reagents administration. Mice were immobilized using custom made stage on a heating pad to maintain body temperature. A LaVison Biotech intravital multiphoton microscope system, based on Ti:sa laser and OPO laser, equipped with a 16X water immersion objective (NA 0.95; Carl Zeiss, Germany) was used to visualize the mouse calvarium and to acquire images. For visualizing of *Pf4-Cre*(+) /Confetti/ *Lyz2*-eGFP mice following laser settings were used: Ti:sa laser (wavelength 800 nm) and an OPO system (wavelength 1050 nm). For clarity MKs are shown single colored in red representing the brightest color in this imaging setup. For the dual antibody labeling setup, a Ti:sa laser (wavelength 840 nm) was used. The vasculature was visualized after i.v. injection of 15 μL Qtracker705 following excitation by Ti:sa laser (wavelength 800 nm). For 4-dimensional image acquisition, image stacks were acquired by capturing a region of interest of $405 \times 405 \mu m^2$ with 2 μm thick imaging layers over a total depth of 40–50 μm every 60 seconds over 1 h. Original image data was processed by IMARIS software (Bitplane).

Time lapse imaging of MK-neutrophil interactions *in vitro*

Neutrophil plucking in co-culture was visualized over a period of at least 3 hours by a Brightfield and Phase Contrast Microscopy (Zeiss, Axiovert 200) with time-lapse images acquisition every 60 seconds. ImageJ software was used for movie generation.

Adoptive neutrophil transfer

Neutrophils were isolated from the BM as described before. Next, 2.5×10^6 neutrophils were injected i.v. into the recipient mice. After one hour, recipient mice were anaesthetized, sacrificed and perfused with PBS and 4% PFA. Bones were embedded in tissue-tek before stored at −20°C.

Adoptive neutrophil transfer in *Mrp8-cre*(+)/iDTR mice

Neutropenia was induced in *Mrp8-cre* (+) iDTR mice as described before. Neutrophil plucking was visualized by multiphoton intravital microscopy over one hour before and after transfer of 2.5×10^6 neutrophils labeled with Ly6G-PE (1: 50, clone 1A8).

Bone whole-mount staining

Frozen, tissue-tec embedded bones (i.e. tibia, humeri) were cut horizontally using a CryoStar NX70 cryotome (Lecia). Bones were immersed in a small tube with blocking buffer (10% goat serum, 3%BSA, 0.5% Triton-X100) at 4°C overnight. Bones were then incubated in the staining solution containing an anti-CD144-biotin and an anti-GFP antibody for 6–8 hours at 4°C. For the secondary antibody staining, bones were washed and incubated in a secondary antibody solution (i.e. streptavidin eFluor450, goat anti-rabbit Alexa488 and CD41-PE) at 4°C overnight. For confocal 3D imaging, bones were immobilized in a plastic sample holder. 3D images were acquired using an inverted Zeiss LSM 880 Airyscan confocal microscope with a plan-Apochromat 100x/1.46 oil-immersion objective and auto-imaging system (Zeiss). Picture analysis was done by using IMARIS software (Bitplane).

Immunofluorescent staining

For MK staining, fetal liver-derived MKs were seeded on coverslips coated with 100 ng/mL fibrinogen for 6 hours in DMEM medium (10% FCS and 1% penicillin/streptomycin) at 37°C and 5% CO_2. Cells then were fixed with 4% PFA for 10 min. After a three-times PBS washing step, MKs were blocked and permeabilized with a blocking solution containing 10% goat serum and 0.5% Triton-X100 for 1 hour at RT. SDF-1 was stained with anti-mouse SDF-1 alpha purified antibody (R&D systems). MKs and nuclei were labeled by an anti-mouse CD41-FITC antibody and Hoechst 33342, respectively.

ROS quantification

ROS amounts were determined in neutrophils isolated from murine BM. Neutrophils were stimulated with 50 nM phorbol 12-myristate 13-acetate (PMA) or 200 ng/mL SDF-1 + 50 nM PMA for 1 h at RT. Cells were subsequently stained with 10 nM 2′,7′-Dichlorodihydrofluorescein diacetate (DCFDA) for 30 min before flow cytometric analysis. For negative control, equal number of neutrophils received same DCFDA staining procedure without prior stimulation.

ROS visualization *in vitro*

Co-cultured cells were stained with 10 nM ′,7′-Dichlorodihydrofluorescein diacetate (DCFDA) for 30 min before being fixed (4% PFA), three times washed with PBST(0.5% tween 20), and stained with Ly6G-PE (1A8) for 30 min. Nuclei were counterstained with DAPI for 5 min at RT. ROS fluorescence was imaged using a Zeiss Axio Observer fluorescent microscopy equipped with 20X objective. Images were analyzed by IMARIS software.

Murine BM cytokine profile analysis

After induction of neutropenia by Gr-1 or control antibody treatment, two tibia and femur bones were isolated. Bones were centrifuged and flushed with 400 μL PBS as described before to wash out BM interstitial fluid. Cytokine amounts were analyzed using a murine proteome cytokine array kit (R&D system, cat#ARY028) according to the manufacture's instruction. Briefly, 200 μL BM

samples were mixed with 15 μL detection cocktail antibody and incubated on a membrane for 1 hour at RT. Next, membranes were incubated with streptavidin-HRP for 30 min at RT. For signal detection, ECL chemiluminescence substrate was added and specific chemiluminescence signals on the membrane were visualized by X-ray film exposure. Relative signal strengths (mean gray intensity compared to reference signal) of each dot were determined by densitometry using ImageJ software.

Acute myocardial infarction mouse model

Male 12- to 20-week old mice were subjected to 1 hour occlusive ligation of left anterior descending (LAD) coronary artery or a sham operation without ligation. Briefly, anesthetized mice were placed on the heat pad to maintain body temperature. Afterward trachea was exposed, a tube connected with ventilator was placed into the trachea to keep mouse respiration rate (RR) at 150/min. Chest cavity was opened at the site between 3rd and 4th ribs and the LAD artery was exhibited by carefully removing pericardium. Thereafter an 8-0 silk suture was slowly passed under the LAD 2–3 mm below left atria avoiding to tear heart tissue. The ligature was closed for one hour. For sham-operated mice, the suture was slowly pulled under the LAD without ligation. After one hour, the ligature was carefully released from the LAD. The chest cavity, muscle and skin layer were closed with a 5-0 suture afterward. All operated mice were kept in a clean cage with heat pad for 48 hours and thereafter used for further investigations.

Ferric(III) chloride-induced thrombus formation in the murine carotid artery model

In anesthetized mice the right common carotid artery was surgically prepared and vessel injury was induced by application of FeCl$_3$ (1 μL of 10% FeCl$_3$ soaked in 1 mm^2 Whatman paper) for 2 min. For intravital microscopy, platelets were labelled by injection of a fluorescently labelled non-blocking platelet antibody (anti-mouse-GPIb-X488, Emfret, 0.5 μg/g body weight) before application of FeCl$_3$. Vessel injury-induced thrombus formation was monitored and imaged for 60 min by *in vivo* video fluorescence microscopy (Axio Zoom.V16 Zeiss microscope equipped with a Zeiss AxioCam). Vessel occlusion was defined as complete cessation of blood flow for at least 10 seconds. Thrombus size was calculated from single images using ImageJ software.

Platelet recruitment into Fe(III) chloride-induced mesenteric artery thrombosis

Single cell imaging of platelet recruitment into thrombi *in vivo* was investigated in murine mesenteric arterioles after vessel injury using FeCl$_3$. In anesthetized mice the mesentery was surgically prepared and mounted on a custom-made stage for intravital microscopy. After the surgical preparation of the mouse mesentery, 3–5 arterioles were chosen and 1% FeCl$_3$ was applied for 10 seconds. To selectively identify freshly released platelets a fluorescently labelled non-blocking platelet antibody (anti-mouse-GPIb-X649, Emfret, 0.5ul/g body weight) was applied 12 hours before the experiment and the same antibody but with different fluorochrome (anti-mouse-GPIb-X488, Emfret, 0.5 μg/g body weight) was applied shortly before the experiment. Accordingly, newly produced platelets within the last 12 hours were single positive while all other platelets were positively stained for both fluorochromes. Intravital fluorescence microscopy was performed using a confocal microscope Zeiss LSM 880 with airyscan microscope. Images were recorded digitally with a Zeiss AxioCam) and analyzed with ImageJ software.

Venous thrombosis model by flow restriction in the vena cava inferior

After a median laparotomy the vena cava inferior (IVC) was exposed and a space holder was positioned followed by a narrowing ligature. Subsequently, the wire was removed to avoid complete vessel occlusion. Side branches were not ligated or manipulated. All groups were age, sex, and weight matched. Mice with bleedings or any injury of the IVC during surgery were excluded from further analysis. For thrombus weight measurement after 48 hours, the IVC was excised just below the renal veins and proximal to the confluence of the common iliac veins.

LPS model

Inflammation was induced by a single intraperitoneal injection of 0.1 mg/kg (bodyweight) LPS as done before (Aslam et al., 2006).

Generation of bone marrow chimera

Bone marrow chimeras were generated by injecting 6x10^6 bone marrow cells isolated from *Cybb*$^{-/-}$ deficient mice (Pollock et al., 1995) into lethally irradiated 8 weeks old CD45.1 recipient mice as done before (Petzold et al., 2013).

Human samples

Acute ST-elevation myocardial infarction (symptom onset <12 h) patients were recruited after giving informed consent at the Heinrich-Heine University (HHU) in Düsseldorf, Germany. All STEMI patients underwent cardiac catheterization with percutaneous coronary intervention. Patients received standard of care medication at the discretion of the interventionalist. 24 h and 5 days after PCI patient blood was drained and analyzed using a blood counter and a BD FACSVerse flow cytometer to determine reticulated platelet fraction and CXCR4 expression on neutrophils. Reticulated platelets were stained with thiazole-orange as described above. Respective control patients with stable coronary artery disease were recruited in the department of cardiology at HHU after giving informed consent. All experiments were approved by the ethics committee of the HHU.

QUANTIFICATION AND STATISTICAL ANALYSIS

Data were analyzed using Prism8 (GraphPad). Normality testing was done using D'Agostino-Pearson omnibus test, where applicable, or Kolmogorov-Smirnov test. Depending on normality distribution, unpaired two-sided Student's *t* test or Mann-Whitney test were used. In matched-sampled experiments, paired Student's *t* test was performed. Tukey-HSD test for one-way ANOVA or two-way ANOVA was used for statistical analysis in multi-group comparison for normal distributed data (Kolmogorov-Smirnov-test), otherwise Kruskal–Wallis- or Wilcox-rank-sum-tests were applied. Correlation analysis was performed using Pearson correlation coefficient test.

GWAS analysis

Vuckovic et al. (Vuckovic et al., 2020) reported a large GWAS on blood cell trait in European cohorts. In these analyses they identified common and rare variants associated with four platelet indices (PLT - Platelet count, MPV - Mean platelet volume, PDW - Platelet distribution width, PCT - Plateletcrit). A GWAS with the sample size N = 408,112 participants of European ancestry was carried out for the UK Biobank. Genome-wide genotyping was performed on all UK Biobank participants using the UK Biobank Axiom Array. More than 90 million variants were imputed using the Haplotype Reference Consortium and UK10K + 1000 Genomes reference panels. Association analyses were then conducted using a linear mixed effects model in order to account for known or cryptic relatedness with the additive genetic model. Details on quality control and statistical methods can be found in Vuckovic et al. (Vuckovic et al., 2020). Summary statistics for platelet traits are available to download from: ftp://ftp.sanger.ac.uk/pub/project/humgen/summary_statistics/UKBB_blood_cell_traits. We used this resource to look up our 20 candidate genes in four platelet indices. We identified all single nucleotide polymorphisms (SNP) and their results in the GWAS within the candidate gene and 50 kb upstream and downstream from the gene. Then we identified the SNP with minimal p-value. Finally, we visually checked local association plots and LD-blocks to see if the block covered the candidate gene. In some cases it was necessary to assign more than one gene to a gene cluster. Then we designated the SNP as sentinel SNP and reported it in Table 1 and Table S1. We used the software SNiPA v3.3 (June 2018, Genome assembly: GRCh37.p13, Ensembl version: 87, 1000 genomes: phase 3 version 5) and R version 3.5.2 to implement this strategy.